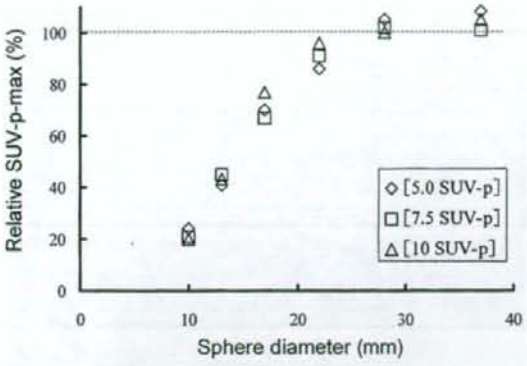

Fig. 2 Relative mean measured standardized uptake value (SUV)-p-max of six spheres for each source-to-background (S/B) ratio. For spheres (less than 22 mm), the measured SUV-p-max decreased dependent on the size of the sphere

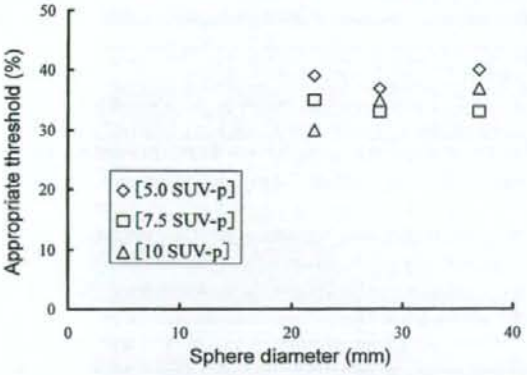

Fig. 3 Appropriate threshold values for each S/B ratio. For spheres (22 mm or more), appropriate threshold values were relatively constant independent of the S/B ratio ranging from 30% to 40% of the measured SUV-p-max

maximum ^{18}FDG activity was inaccurate because of the partial volume effect. Thus, we analyzed only spheres of 22 mm or more in the subsequent experiments.

Figure 3 is a plot of appropriate threshold values of spheres of 22 mm, 28 mm, and 37 mm for each S/B ratio. The appropriate threshold values ranged from 30% to 40% of the SUV-p-max, independent of the S/B ratio. Therefore, we adopted a threshold value of 35% of the measured SUV-p-max.

Figure 4 shows the averages of the measured SUV-p-max of spheres of 22 mm, 28 mm, and 37 mm for an S/B ratio of 20 in moving phantom experiments. For a sphere of 37 mm, the measured SUV-p-max did not decrease

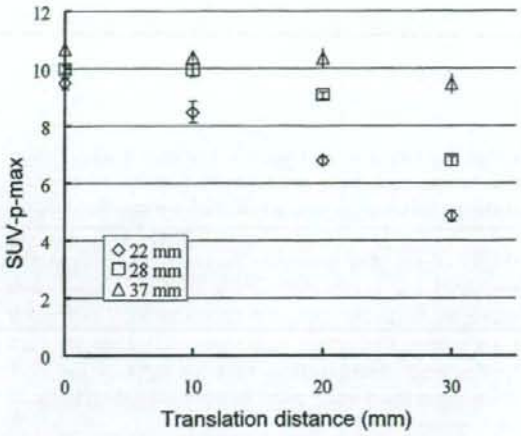

Fig. 4 Averages and standard deviations of the measured maximum [^{18}F] fluoro-2-deoxyglucose activity for spheres of 22 mm, 28 mm, and 37 mm in moving phantom experiments. For spheres of 22 mm and 28 mm, the measured SUV-p-max decreased significantly dependent on the translation distance

significantly, and ranged from 9.5 to 10.4 SUV-p. But for spheres of 22 mm and 28 mm, the measured SUV-p-max decreased significantly dependent on the translation distance.

CT and PET images

Examples of delineation with CT and PET are shown in Fig. 5. Figure 5a, b shows an anterior–posterior digitally reconstructed radiograph (DRR) image of a sphere of 28 mm from CT images in the static and moving phantom experiments. The DRR image of a static sphere is circular and smooth, but that of a moving sphere is distorted. For a moving sphere, two separate elliptical CT images were generated in some cases. In such cases, maximum sizes delineated by CT were measured from the top of the upper ellipse to the bottom of the lower ellipse. Figure 5c, d shows an anterior–posterior DRR image of a sphere of 28 mm from PET images depicted with a threshold value of 35% in static and moving phantom experiments. The DRR image of a static sphere is a circle, but that of a moving sphere is delineated lengthwise and an oval.

The averages of the maximum size of CT and PET delineation of spheres of 22 mm, 28 mm, and 37 mm in both the axial and sagittal planes are shown in Table 2. In the axial plane, all sizes of CT delineation were smaller than the actual sphere size, with a difference of 0.4–1.2 mm. In the sagittal plane, sizes of CT delineation

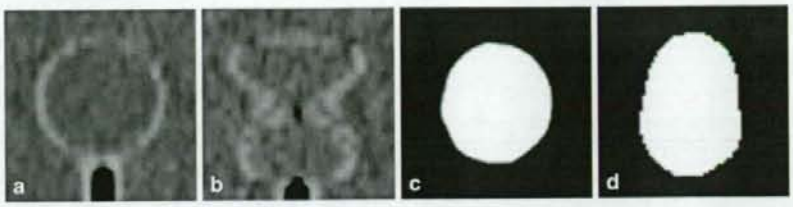

Fig. 5 Digitally reconstructed radiographs (DRRs) of a 28-mm-diameter sphere generated from computed tomographic (CT) images and positron emission tomographic (PET) images in a sagittal plane. The total translation in the moving experiment was 20 mm. **a, b** DRRs of CT images generated from static and moving sphere images, respectively. A DRR image of a static sphere is circular and smooth, but that of a moving sphere is distorted. **c, d** DRRs of PET images generated from static and moving sphere images, respectively. A DRR image of a static sphere is a circle, but that of a moving sphere is delineated lengthwise and an oval

Table 2 The averages of the maximum diameter of static and moving spheres on PET and CT images

Sphere size (mm)	Translation (mm)	Diameter of PET/CT images (mm)		Difference between PET/CT and actual diameter (mm)	
		PET image[a]	CT image[a]	PET image[a]	CT image[a]
Axial plane					
22	10	22.4 ± 1.1	21.4 ± 0.5	0.4	0.6
	20	22.0 ± 0.7	21.2 ± 0.4	2.0	0.8
	30	22.8 ± 0.8	20.8 ± 1.1	0.8	1.2
28	10	27.8 ± 0.4	27.6 ± 0.5	0.2	0.4
	20	25.8 ± 0.4	27.0 ± 0	2.2	1.0
	30	26.2 ± 1.3	27.2 ± 0.8	1.8	0.8
37	10	37.2 ± 0.4	36.6 ± 0.5	0.2	0.4
	20	35.0 ± 0	36.2 ± 0.4	2.0	0.8
	30	33.8 ± 0.4	36.4 ± 0.5	3.2	0.6
Sagittal plane					
22	10	24.2 ± 0.4	16.6 ± 6.9	7.8	15.4
	20	31.4 ± 1.1	17.8 ± 11.6	10.6	24.2
	30	43.4 ± 0.9	31.8 ± 1.8	8.6	29.8
28	10	29.8 ± 0.4	22.6 ± 5.7	8.2	15.4
	20	35.2 ± 0.8	27.4 ± 8.6	12.8	20.6
	30	44.8 ± 1.8	33.6 ± 1.7	13.2	24.4
37	10	39.0 ± 0.7	38.6 ± 2.2	8.0	8.4
	20	44.2 ± 0.8	44.4 ± 11.7	12.8	12.6
	30	51.0 ± 1.9	40.6 ± 12.0	16.0	26.4

PET positron emission tomography, *CT* computed tomography
[a]Averages and standard deviations of the maximum size from five measurements

deviated significantly with large standard deviations (SDs). The difference between the average sizes of CT delineation and the corresponding real ITV (an actual sphere diameter plus moving distance) ranged from 8.4 mm to 29.8 mm.

In the axial plane, the sizes of PET delineation tended to be smaller than the actual sphere sizes, whereas in the sagittal plane all sizes of PET delineation were larger than the actual sphere sizes and increased dependent on the translation distance with small SDs. However, these values were smaller than the real ITV, and the difference between the average sizes of PET delineation and the real ITV ranged from 7.8 mm to 16.0 mm.

Discussion

Table 1 summarizes the various thresholds for the target delineation with PET proposed by various investigators. Although there are many reports on this matter, most reports are based on static phantom experiments or a limited number of patients. Of the three reports using moving phantoms, two are basic experiments for respiratory gating 4D-PET images. Only one study described the benefit of PET images in delineating ITV [23]. However, appropriate threshold values for moving phantoms have never been reported. In the present phantom experiments, the PET delineations with a 35%

threshold fitted well to the actual spheres from 22 mm to 37 mm in an axial plane for both static and moving phantoms.

In several studies, the target was delineated by PET using a simple threshold, a percentage of the maximum FDG activity [21–25]. In other studies, a complex threshold computed from the mean activity of a target and background was used [26–28]. However, a standardized method for optimal PET delineation in RTP has not yet been established. Recently, several investigators have reported that the use of a single-threshold model for delineating the GTV with PET/CT is not sufficient because of the effects of the target size, motion, and image reconstruction parameters [29, 30]. For example, Biehl et al. [30] reported that the threshold for delineating the target should be changed dependent on the target size. Thus, we consider that a threshold of 35% of measured maximum FDG activity is only a provisional criterion for small tumors of 2–4 cm, and adjustment of the threshold is required for larger tumors in the clinical setting.

As one notable finding of the present study, the measured maximum FDG activity of the spheres decreased significantly dependent on the translation distance. Although this result is quite reasonable on the basis of an understanding of the characteristics of radioactivity measurement, to our knowledge there are no prior reports on this finding. Sasaki et al. [36] reported that the maximum FDG activity of the target is a strong prognostic factor for NSCLC regardless of whether curative surgery or radiation treatment is undertaken. They suggested that tumors with high FDG activity have the potential to be resistant to cancer therapy. However, our experiments demonstrated that the maximum FDG activity decreased according to the size and motion distance of spheres. As the maximum FDG activity can be changed dependent on the size and motion of tumors, absolute values do not necessarily represent biological features of tumor cells.

Recently, RTP using four-dimensional CT (4D-CT) has been investigated to improve target delineation [37–39]. Certainly, 4D-CT can provide more accurate delineation of moving targets, and comparison between PET images and 4D-CT is desirable. However, at present, the availability of RTP on the basis of 4D-CT is limited to only a few advanced institutions in the world, and RTP is performed by using conventional CT images at most institutions. In addition, our PET/CT system does not correspond to 4D-CT. For the above reasons, we compared PET images with conventional CT images.

Computed tomographic-based targets in moving phantom experiments were distorted and/or separated (Fig. 5b). These distortions have the potential to cause a geographic misalignment. However, PET-based targets in the moving phantom experiments were smooth and elliptical in the sagittal view, and the diameter increased dependent on the translation distance (Fig. 5d). Because they take a few minutes to acquire, PET images include numerous respiratory cycles. Thus, elliptical PET-based targets in a sagittal plane include ITV and can eliminate the geographic error [23].

The present results suggest that PET has the potential to provide individual ITVs. However, the diameters of PET-based targets were smaller than the real ITV including the actual sphere plus movement distance in the translation direction. Therefore, in RTP with PET/CT, the PTV margin for the sagittal direction should be larger than that for the axial direction. As this study was performed using a phantom with a known size and motion distance, clinical validation for appropriate PTV margins will be required.

Conclusions

When a threshold value of 35% of the measured maximum FDG activity was adopted, the sizes of PET images were almost the same for static and moving phantom spheres of 22 mm, 28 mm, and 37 mm in the axial plane. As appropriate threshold values can be changed on the basis of the tumor size, the threshold of 35% of measured maximum FDG activity is only a provisional criterion for tumors of 2–4 cm, and adjustment of the threshold may be required for larger tumors in the clinical setting. In addition, sizes of PET delineation in the sagittal plane were larger than the actual sphere and increased dependent on the translation distance, indicating that PET images have the potential to provide an individualized ITV. Thus, PET/CT simulation seems to provide a strong benefit for lung tumors.

Acknowledgments This study was supported in part by a Grant-in-Aid for Scientific Research (17591300) from the Ministry of Education, Culture, Sports, Science and Technology, Japan, and by a Grant-in-Aid in 2006 from the Association for Nuclear Technology in Medicine.

References

1. Mac Manus MP, Wong K, Hicks RJ, Matthews JP, Wirth A, Ball DL. Early mortality after radical radiotherapy for non-small-cell lung cancer: comparison of PET-staged and conventionally staged cohorts treated at a large tertiary referral center. Int J Radiat Oncol Biol Phys 2002;52:351–61.
2. Viney RC, Boyer MJ, King MT, Kenny PM, Pollicino CA, McLean JM, et al. Randomized controlled trial of the role of positron emission tomography in the management of stage I

and II non-small-cell lung cancer. J Clin Oncol 2004;22: 2357–62.
3. Bradley JD, Dehdashti F, Mintun MA, Govindan R, Trinkaus K, Siegel BA. Positron emission tomography in limited-stage small-cell lung cancer: a prospective study. J Clin Oncol 2004;22:3248–54.
4. Koike I, Ohmura M, Hata M, Takahashi N, Oka T, Ogino I, et al. FDG-PET scanning after radiation can predict tumor regrowth three months later. Int J Radiat Oncol Biol Phys 2003;57:1231–8.
5. Lehtiö K, Eskola O, Viljanen T, Oikonen V, Grönroos T, Sillanmäki L, et al. Imaging perfusion and hypoxia with PET to predict radiotherapy response in head-and-neck cancer. Int J Radiat Oncol Biol Phys 2004;59:971–82.
6. Hernandez-Maraver D, Hernandez-Navarro F, Gomez-Leon N, Coya J, Rodriguez-Vigil B, Madero R, et al. Positron emission tomography/computed tomography: diagnostic accuracy in lymphoma. Br J Haematol 2006;135:293–302.
7. Votrubova J, Belohlavek O, Jaruskova M, Oliverius M, Lohynska R, Trskova K, et al. The role of FDG-PET/CT in the detection of recurrent colorectal cancer. Eur J Nucl Med Mol Imaging 2006;33:779–84.
8. Yuan S, Yu Y, Chao KS, Fu Z, Yin Y, Liu T, et al. Additional value of PET/CT over PET in assessment of locoregional lymph nodes in thoracic esophageal squamous cell cancer. J Nucl Med 2006;47:1255–9.
9. Antoch G, Saoudi N, Kuehl H, Dahmen G, Mueller SP, Beyer T, et al. Accuracy of whole-body dual-modality fluorine-18-2-fluoro-2-deoxy-D-glucose positron emission tomography and computed tomography (FDG-PET/CT) for tumor staging in solid tumors: comparison with CT and PET. J Clin Oncol 2004;22:4357–68.
10. Keidar Z, Haim N, Guralnik L, Wollner M, Bar-Shalom R, Ben-Nun A, et al. PET/CT using ^{18}F-FDG in suspected lung cancer recurrence: diagnostic value and impact on patient management. J Nucl Med 2004;45:1640–6.
11. Faria SL, Menard S, Devic S, Sirois C, Souhami L, Lisbona R, et al. Impact of FDG-PET on radiation therapy volume delineation in non-small-cell lung cancer. Int J Radiat Oncol Biol Phys 2004;59:78–86.
12. Ciernik IF, Dizendorf E, Baumert BG, Reiner B, Burger C, Davis JB, et al. Radiation treatment planning with an integrated positron emission and computer tomography (PET/CT): a feasibility study. Int J Radiat Oncol Biol Phys 2003;57:853–63.
13. van Der Wel A, Nijsten S, Hochstenbag M, Lamers R, Boersma L, Wanders R, et al. Increased therapeutic ratio by ^{18}FDG-PET CT planning in patients with clinical CT stage N2-N3M0 non-small-cell lung cancer: a modeling study. Int J Radiat Oncol Biol Phys 2005;61:649–55.
14. Heron DE, Andrade RS, Flickinger J, Johnson J, Agarwala SS, Wu A, et al. Hybrid PET-CT simulation for radiation treatment planning in head-and-neck cancers: a brief technical report. Int J Radiat Oncol Biol Phys 2004;60:1419–24.
15. Vrieze O, Haustermans K, De Wever W, Lerut T, Van Cutsem E, Ectors N, et al. Is there a role for FDG-PET in radiotherapy planning in esophageal carcinoma? Radiother Oncol 2004;73:269–75.
16. Nishioka T, Shiga T, Shirato H, Tsukamoto E, Tsuchiya K, Kato T, et al. Image fusion between ^{18}FDG-PET and MRI/CT for radiotherapy planning of oropharyngeal and nasopharyngeal carcinomas. Int J Radiat Oncol Biol Phys 2002;53: 1051–7.
17. Mutic S, Malyapa RS, Grigsby PW, Dehdashti F, Miller TR, Zoberi I, et al. PET-guided IMRT for cervical carcinoma with positive para-aortic lymph nodes—a dose-escalation treatment planning study. Int J Radiat Oncol Biol Phys 2003;55:28–35.
18. Caldwell CB, Mah K, Ung YC, Danjoux CE, Balogh JM, Ganguli SN, et al. Observer variation in contouring gross tumor volume in patients with poorly defined non-small cell lung tumors on CT: the impact of ^{18}FDG-Hybrid PET fusion. Int J Radiat Oncol Biol Phys 2001;51:923–31.
19. Erdi YE, Rosenzweig K, Erdi AK, Macapinlac HA, Hu YC, Braban LE, et al. Radiotherapy treatment planning for patients with non-small cell lung cancer using positron emission tomography (PET). Radiother Oncol 2002;62:51–60.
20. Mah K, Caldwell CB, Ung YC, Danjoux CE, Balogh JM, Ganguli SN, et al. The impact of 18 FDG-PET on target and critical organs in CT-based treatment planning of patients with poorly defined non-small-cell lung carcinoma: a prospective study. Int J Radiat Oncol Biol Phys 2002;52:339–50.
21. Erdi YE, Mawlawi O, Larson SM, Imbriaco M, Yeung H, Finn R, et al. Segmentation of lung lesion volume by adaptive positron emission tomography image thresholding. Cancer 1997;80:2505–9.
22. Nagel CC, Bosmans G, Dekker AL, Ollers MC, De Ruysscher DK, Lambin P, et al. Phased attenuation correction in respiration correlated computed tomography/positron emitted tomography. Med Phys 2006;33:1840–7.
23. Caldwell CB, Mah K, Skinner M, Danjoux CE. Can PET provide the 3D extent of tumor for individualized internal target volumes? A phantom study of the limitations of CT and the promise of PET. Int J Radiat Oncol Biol Phys 2003;55: 1381–93.
24. Deniaud-Alexandre E, Touboul E, Lerouge D, Grahek D, Foulquier JN, Petegnief Y, et al. Impact of computed tomography and 18F-deoxyglucose coincidence detection emission tomography image fusion for optimization of conformal radiotherapy in non-small-cell lung cancer. Int J Radiat Oncol Biol Phys 2005;63:1432–41.
25. Ford EC, Kinahan PE, Hanlon L, Alessio A, Rajendran J, Schwartz DL, et al. Tumor delineation using PET in head and neck cancers: threshold contouring and lesion volumes. Med Phys 2006;33:4280–8.
26. Nestle U, Kremp S, Schaefer-Schuler A, Sebastian-Welsch C, Hellwig D, Rübe C, et al. Comparison of different methods for delineation of ^{18}FDG-PET-positive tissue for target volume definition in radiotherapy of patients with non-small cell lung cancer. J Nucl Med 2005;46:1342–8.
27. Black QC, Grills IS, Kestin LL, Wong CY, Wong JW, Martinez AA, et al. Defining a radiotherapy target with positron emission tomography. Int J Radiat Oncol Biol Phys 2004;60:1272–82.
28. Davis JB, Reiner B, Huser M, Burger C, Székely G, Ciernik IF. Assessment of ^{18}F PET signals for automatic target volume definition in radiotherapy treatment planning. Radiother Oncol 2006;80:43–50.
29. Yaremko B, Riauka T, Robinson D, Murray B, Alexander A, McEwan A, et al. Thresholding in PET images of static and moving targets. Phys Med Biol 2005;50:5969–82.
30. Biehl KJ, Kong FM, Dehdashti F, Jin JY, Mutic S, El Naqa I, et al. ^{18}F-FDG PET definition of gross tumor volume for radiotherapy of non-small cell lung cancer: is a single standardized uptake value threshold approach appropriate? J Nucl Med 2006;47:1808–12.
31. Hong R, Halama J, Bova D, Sethi A, Emami B. Correlation of PET standard uptake value and CT window-level threshold for target delineation in CT-based radiation treatment planning. Int J Radiat Oncol Biol Phys 2007;67:720–6.
32. Ashamalla H, Rafla S, Parikh K, Mokhtar B, Goswami G, Kambam S, et al. The contribution of integrated PET/CT to

the evolving definition of treatment volumes in radiation treatment planning in lung cancer. Int J Radiat Oncol Biol Phys 2005;63:1016–23.
33. Plathow C, Ley S, Fink C, Puderbach M, Hosch W, Schmähl A, et al. Analysis of intrathoracic tumor mobility during whole breathing cycle by dynamic MRI. Int J Radiat Oncol Biol Phys 2004;59:952–9.
34. Ross CS, Hussey DH, Pennington EC, Stanford W, Doornbos JF. Analysis of movement of intrathoracic neoplasms using ultrafast computerized tomography. Int J Radiat Oncol Biol Phys 1990;18:671–7.
35. Stevens CW, Munden RF, Forster KM, Kelly JF, Liao Z, Starkschall G, et al. Respiratory-driven lung tumor motion is independent of tumor size, tumor location, and pulmonary function. Int J Radiat Oncol Biol Phys 2001;51:62–8.
36. Sasaki R, Komaki R, Macapinlac H, Erasmus J, Allen P, Forster K, et al. [18F]fluorodeoxyglucose uptake by positron emission tomography predicts outcome of non-small-cell lung cancer. J Clin Oncol 2005;23:1136–43.
37. Sarrut D, Boldea V, Miguet S, Ginestet C. Simulation of 4D CT Images from deformable registration between inhale and exhale breath-hold CT scans. Int J Radiat Oncol Biol Phys 2005;63:S509–10.
38. Low DA, Nystrom M, Kalinin E, Parikh P, Dempsey JF, Bradley JD, et al. A method for the reconstruction of four-dimensional synchronized CT scans acquired during free breathing. Med Phys 2003;30:1254–63.
39. Britton KR, Starkschall G, Tucker SL, Pan T, Nelson C, Chang JY, et al. Assessment of gross tumor volume regression and motion changes during radiotherapy for non-small-cell lung cancer as measured by four-dimensional computed tomography. Int J Radiat Oncol Biol Phys 2007;68:1036–46.

IL12RB2 and *ABCA1* Genes Are Associated with Susceptibility to Radiation Dermatitis

Minoru Isomura,[1,6] Natsuo Oya,[7,8] Seiji Tachiiri,[8] Yuko Kaneyasu,[9] Yasumasa Nishimura,[10] Tetsuo Akimoto,[2,11] Masato Hareyama,[12] Tadasi Sugita,[13] Norio Mitsuhashi,[2] Takashi Yamashita,[3] Masahiko Aoki,[15] Heitetsu Sai,[8,14] Yutaka Hirokawa,[4,9] Koh-ichi Sakata,[12] Kumiko Karasawa,[4] Akihiro Tomida,[5] Takashi Tsuruo,[5] Yoshio Miki,[1,6] Tetsuo Noda,[1] and Masahiro Hiraoka[8]

Abstract

Purpose: Severe acute radiation dermatitis is observed in approximately 5% to 10% of patients who receive whole-breast radiotherapy. Several factors, including treatment-related and patient-oriented factors, are involved in susceptibility to severe dermatitis. Genetic factors are also thought to be related to a patient's susceptibility to severe dermatitis. To elucidate genetic polymorphisms associated with a susceptibility to radiation-induced dermatitis, a large-scale single-nucleotide polymorphism (SNP) analysis using DNA samples from 156 patients with breast cancer was conducted.

Experimental Design: Patients were selected from more than 3,000 female patients with early breast cancer who received radiotherapy after undergoing breast-conserving surgery. The dermatitis group was defined as patients who developed dermatitis at a National Cancer Institute Common Toxicity Criteria grade of ≥2. For the SNP analysis, DNA samples from each patient were subjected to the genotyping of 3,144 SNPs covering 494 genes.

Results: SNPs that mapped to two genes, *ABCA1* and *IL12RB2*, were associated with radiation-induced dermatitis. In the *ABCA1* gene, one of these SNPs was a nonsynonymous coding SNP causing R219K ($P = 0.0065$). As for the *IL12RB2* gene, the strongest association was observed at SNP-K (rs3790568; $P = 0.0013$). Using polymorphisms of both genes, the probability of severe dermatitis was estimated for each combination of genotypes. These analyses showed that individuals carrying a combination of genotypes accounting for 14.7% of the Japanese population have the highest probability of developing radiation-induced dermatitis.

Conclusion: Our results shed light on the mechanisms responsible for radiation-induced dermatitis. These results may also contribute to the individualization of radiotherapy.

Breast-conserving therapy, consisting of breast-conserving surgery and prophylactic breast irradiation, is the standard therapy for patients with early breast cancer. In most institutions, a total dose of 45 to 50 Gy is delivered to the whole breast with a daily fraction of 1.8 to 2 Gy; this dose fractionation is regarded to be effective and safe, considering both the excellent local control rate and the low probability of severe radiation-related toxicity (1).

Mild acute radiation dermatitis is commonly observed during or shortly after the completion of radiotherapy. However, large interindividual variations in the severity of dermatitis exist even when the patients have been uniformly irradiated. Approximately 5% to 10% of patients develop moderate to severe acute radiation dermatitis following whole-breast radiotherapy (2, 3).

Variations in the severity of radiation dermatitis are influenced by both treatment-related and patient-related

Authors' Affiliations: [1]Genome Center, Japanese Foundation for Cancer Research; [2]Department of Radiology, Tokyo Women's Medical University, School of Medicine; [3]Department of Radiation Oncology, Cancer Institute Hospital; [4]Department of Radiology, School of Medicine, Juntendo University; [5]Institute of Molecular and Cellular Biosciences, The University of Tokyo; [6]Department of Molecular Genetics, Medical Research Institute, Tokyo Medical and Dental University, Tokyo, Japan; [7]Department of Radiation Oncology, Graduate School of Medical Sciences, Kumamoto University, Kumamoto, Japan; [8]Department of Radiation Oncology and Image-Applied Therapy, Graduate School of Medicine, Kyoto University, Kyoto, Japan; [9]Department of Radiology, Hiroshima University, Hiroshima, Japan; [10]Department of Radiation Oncology, Kinki University School of Medicine, Osaka, Japan; [11]Department of Radiation Oncology, Gunma University Graduate School of Medicine, Maebashi, Japan; [12]Department of Radiology, Sapporo Medical University, School of Medicine, Sapporo, Japan; [13]Department of Radiology, Niigata Cancer Center Hospital; [14]Department of Radiology, Niigata University Graduate School of Medical and Dental Sciences, Niigata, Japan; and [15]Department of Radiology, Hirosaki University School of Medicine, Hirosaki, Japan

Received 9/13/07; revised 4/19/08; accepted 4/21/08.

Grant support: Japanese Millennium Project.

The costs of publication of this article were defrayed in part by the payment of page charges. This article must therefore be hereby marked *advertisement* in accordance with 18 U.S.C. Section 1734 solely to indicate this fact.

Note: Supplementary data for this article are available at Clinical Cancer Research Online (http://clincancerres.aacrjournals.org/).

M. Isomura and N. Oya contributed equally to this work.

Requests for reprints: Yoshio Miki, Genome Center, Japanese Foundation for Cancer Research, 3-10-6 Ariake, Koto-ku, Tokyo 135-8550, Japan. Phone: 81-3-3570-0453; Fax: 81-3-3570-0454; E-mail: miki@jfcr.or.jp.

doi:10.1158/1078-0432.CCR-07-4389

factors. Treatment-related factors include radiotherapy variables (e.g., beam energy, radiation dose, dose fractionation, overall treatment time, heterogeneity in dose distribution, and concurrent chemotherapy). Hotspots produced by radiation dose heterogeneity often result in focally enhanced dermatitis. Patient-related factors include patient age, menopausal state, physique, and coexistent diabetes mellitus or collagen disease. In addition, several genetic syndromes such as ataxia telangiectasia (4, 5), Fanconi anemia (6, 7), and Nijmegen breakage syndrome (8, 9) have been reported to account for a small, but prominent, percentage of the hyperradiosensitive population.

In the majority of patients with moderate to severe radiation dermatitis, however, the cause of the radiosensitivity is unknown, implying the existence of undetermined intrinsic factors (10). Establishing a system for predicting patients with intrinsic radiosensitivity before subjecting them to conventional radiotherapy would be clinically useful for the individualization of radiotherapy and, consequently, for improving the treatment outcome.

The aim of the present study was to identify radiation dermatitis-related single-nucleotide polymorphisms (SNP) using peripheral lymphocytes from patients who developed radiation dermatitis after whole-breast irradiation.

Materials and Methods

Patient selection and study design. A multi-institutional, case-control study comprehensively analyzing SNPs and comparing alleles between control patients and patients who were considered to have intrinsic radiosensitivity was conducted. This study was approved by the institutional review board of each institution involved in the study. Candidate patients were selected from a pool of more than 3,000 female patients who had undergone whole-breast radiotherapy following breast-conserving surgery for the treatment of early breast cancer since June 1993 at nine institutions. The eligibility criteria were as follows: (*a*) patients who had undergone a quadrantectomy or wide excision for unilateral early breast cancer, (*b*) patients who had received traditional tangential whole-breast irradiation at a total radiation dose of 44 to 52 Gy at a daily fraction of 1.8 to 2.2 Gy over a period of less than 8 wk using a cobalt-60 source or a linear accelerator generating 4 to 6 MV X-rays, (*c*) patients whose radiation dose distribution was available, (*d*) patients who did not receive systemic chemotherapy or hormonal therapy except for oral fluorouracil or tamoxifen during the radiotherapy period, and (*e*) patients whose skin reactions were followed-up for at least 6 mo after the completion of radiotherapy.

The severity of dermatitis was graded according to the National Cancer Institute Common Toxicity Criteria. The dermatitis group in the present study was regarded to represent patients with intrinsic hypersensitivity. Clinical records, photographs of the skin before and after irradiation, and the radiation dose distribution charts were carefully reviewed to exclude confounding external factors. To exclude patients with treatment-related dermatitis, patients with focal dermatitis that could be explained by comparing the dose distribution and the dermatitis distribution to reveal focal hotspots or focal boost irradiation were strictly excluded from the present study. For example, localized dermatitis of grade ≥2 that was limited to the axilla, the submammary fold, or the nipple was regarded as indicating ineligibility for inclusion in the dermatitis group. Only patients with acute radiation dermatitis of grade ≥2 distributed evenly over the irradiated skin were regarded as having intrinsic radiosensitivity and were included in the dermatitis group.

The control group was determined by selecting patients from the pool of patients who developed grade 0 to 1 dermatitis. Patient-to-patient matching between the dermatitis group and the control group was used to ensure that the two groups would be well balanced in terms of their major characteristics and therapeutic variables. The matched factors included the patients' ages, menopausal states, use of concurrent oral fluorouracil, institution where the radiotherapy was done, radiation dose fractionation, radiation quality, and the year of radiotherapy. Two typical cases from the dermatitis group and a case from the control group are shown in Fig. 1.

Between September 2001 and September 2003, 77 patients in the dermatitis group and 79 patients in the control group were interviewed to confirm their eligibility for enrollment in the study; 15 mL of peripheral venous blood were then drawn after obtaining the patient's written informed consent.

Single-nucleotide polymorphisms. To identify polymorphisms associated with radiation dermatitis, 494 genes were selected for analysis (Table 1). These genes included DNA repair genes, apoptosis-related genes, inflammation-related genes, angiogenesis-related genes, and transporter genes. We then searched for SNPs located within or close to these genes using the JSNP database (11). A total of 3,144 SNPs were selected for genotyping. A complete list of the SNPs used in the present study is available on our Internet web page (URL to be updated).

Genotyping. After informed consent was obtained, 15 mL of peripheral blood were obtained from each patient. DNA was extracted from mononuclear cells using standard methods. Genotyping was done according to the high-throughput SNP typing method developed at Riken (12). Fluorescent signals were detected using Tecan Ultra (Tecan Group Ltd.). The genotypes were determined using automated genotyping software (13).

Statistical analysis. The associations between the SNPs and radiation dermatitis were examined using a test for independency with a 2×3 contingency table, in which the two distributions corresponded to patients with and those without radiation dermatitis. As we had already selected candidate genes that we suspected to be associated with radiation dermatitis, the SNPs were searched for in a manner that minimized the chance of missing any SNP associated with dermatitis. For this reason, the cutoff point was set at $P < 0.01$. We selected a locus when multiple SNPs mapped to that region were associated with radiation dermatitis at a P value smaller than the cutoff value. After

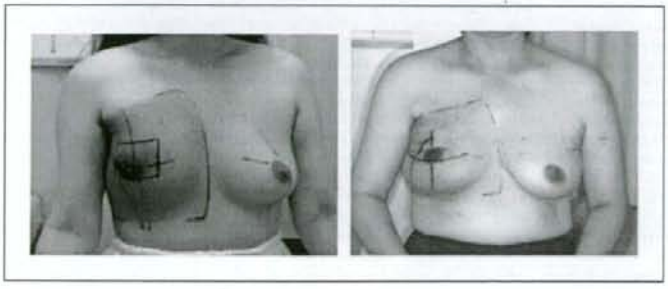

Fig. 1. Two typical cases from the dermatitis group and a case from the control group. Left, dermatitis group; right, control group.

Table 1. List of genes investigated in this study

ABCA1	*BIRC4*	*CD28*	*CYP2A6*	*FGF2*	*IL13RA2*	*MSH4*	*RAD18*	*SP1*	*TOP3B*
ABCA4	*BIRC5*	*CDA*	*CYP2A7*	*FLT1*	*IL14*	*MSH6*	*RAD23A*	*STAT1*	*TP73*
ABCA5	*BIRC6*	*CDC2*	*CYP2B6*	*FMO1*	*IL16*	*MT1H*	*RAD50*	*STAT4*	*TP73L*
ABCB1	*BIRC7*	*CDC25A*	*CYP2C18*	*FMO5*	*IL17*	*MTF1*	*RAD51*	*STAT5A*	*TRAF1*
ABCB11	*BIRC8*	*CDC25B*	*CYP2C8*	*FOS*	*IL18BP*	*MTHFR*	*RAD51L1*	*STAT6*	*TRAF5*
ABCB4	*BLM*	*CDC25C*	*CYP2C9*	*G22P1*	*IL18R1*	*MUTYH*	*RAD51L3*	*STE*	*TTRAP*
ABCC1	*BLR1*	*CDK1B*	*CYP2D6*	*GADD45A*	*IL19*	*MVP*	*RAD52*	*SULT1A2*	*TUBA1*
ABCC2	*BMPR1B*	*CDK2*	*CYP2E*	*GATA3*	*IL1A*	*MYC*	*RAD54L*	*SULT1A3*	*TUBA2*
ABCC3	*BMPR2*	*CDK3*	*CYP3A4*	*GCLC*	*IL1B*	*NAT2*	*RAD9A*	*SULT1B1*	*TUBA3*
ABCC4	*BRAP*	*CDK4*	*CYP3A5*	*GCLM*	*IL1R1*	*NBS1*	*RAF1*	*SULT1C1*	*TUBA4*
ABCC5	*BRCA1*	*CDK5*	*CYP3A7*	*GPR81*	*IL1R2*	*NDRG1*	*RASA1*	*SULT2A1*	*TUBB5*
ABCC6	*BRCA2*	*CDK6*	*CYP7A1*	*GPX2*	*IL2*	*NEIL2*	*RB1*	*SULT2B1*	*TYMS*
ABCG1	*BUB1B*	*CDK7*	*CYP7B1*	*GPX3*	*IL27w*	*NF1*	*RBL1*	*TAP2*	*UGT1*
ABCG2	*BUB3*	*CDKN1A*	*DAXX*	*GPX4*	*IL2RA*	*NFATC2*	*RBL2*	*TBP*	*UGT1A9*
ABL1	*CASP10*	*CDKN1B*	*DCK*	*GSK3B*	*IL3*	*NFATC3*	*RECQL5*	*TBX21*	*UGT2A1*
ABL2	*CASP3*	*CDKN1C*	*DCLRE1A*	*GSR*	*IL4*	*NFATC4*	*RFC1*	*TCP10*	*UGT2B15*
ADH1A	*CASP6*	*CDKN2A*	*DCLRE1B*	*GSTM1*	*IL4R*	*NFKB1*	*RPA1*	*TDG*	*UGT2B4*
ADH1B	*CASP7*	*CDKN2C*	*DCLRE1C*	*GSTM3*	*IL5RA*	*NFKB2*	*RPA2*	*TDGF1*	*UMPK*
ADH1C	*CASP8*	*CDKN2D*	*DCTD*	*GSTP1*	*IL6*	*NFKBIL1*	*RPA3*	*TEAD1*	*UMPS*
ADH4	*CASP9*	*CDKN3*	*DDB2*	*GSTT1*	*IL8RB*	*NME1*	*RRM1*	*TERF1*	*VEGF*
ADH6	*CAT*	*CER1*	*DDR1*	*H2AFX*	*IL9*	*NQO1*	*RUVBL2*	*TERT*	*VEGFB*
ADPRT	*CCBP2*	*CES1*	*DHFR*	*HAVCR2*	*IRF1*	*NQO2*	*SIRT1*	*TFDP1*	*VEGFC*
ADPRTL2	*CCL1*	*CES2*	*DMC1*	*HIF1A*	*ITGB2*	*NRP1*	*SLC10A1*	*TFDP2*	*WEE1*
ADPRTL3	*CCL11*	*CFLAR*	*DPYD*	*HM74*	*JAK1*	*NUMB*	*SLC15A1*	*TGFB1*	*WRN*
ALDH1A1	*CCL13*	*CHEK1*	*DRD2*	*HMOX1*	*JAK3*	*OAT*	*SLC15A2*	*TGFB1I1*	*WT1*
ALDH3A1	*CCL15*	*CHEK2*	*DUT*	*HMOX2*	*KDR*	*ODC1*	*SLC16A1*	*TGFB2*	*XAB2*
ALDH3A2	*CCL17*	*CHUK*	*E2F1*	*HNK-1ST*	*KIAA1821*	*PCAF*	*SLC17A4*	*TGFB3*	*XCL1*
ALDH3B1	*CCL18*	*CIP1*	*E2F2*	*HSPA1B*	*KITLG*	*PCNA*	*SLC21A11*	*TGFBI*	*XCL2*
ALDH3B2	*CCL2*	*CKN1*	*E2F3*	*HSPA2*	*LIG1*	*PDGFB*	*SLC21A12*	*TGFBR1*	*XPA*
ALDH9A1	*CCL22*	*COMT*	*E2F5*	*HSPA5*	*LIG3*	*PDGFRB*	*SLC21A3*	*TGFBR2*	*XPC*
AMHR2	*CCL24*	*CREBBP*	*EGF*	*HSPA8*	*LRDD*	*PEMT*	*SLC21A6*	*TGFBR3*	*XRCC1*
APAF1	*CCL25*	*CRYAB*	*EGFR*	*HSPA9B*	*MAD1L1*	*PGF*	*SLC21A8*	*TH1L*	*XRCC2*
ATIC	*CCL26*	*CSF1*	*EP300*	*HSPCA*	*MAD2L1*	*PIG3*	*SLC21A9*	*THBS1*	*XRCC3*
ATM	*CCL28*	*CSF3*	*EPHX1*	*HSPCB*	*MAD2L2*	*PIK3C2B*	*SLC22A1*	*THRA*	*XRCC4*
ATP1A2	*CCL3*	*CSNK1A1*	*EPHX2*	*HTFR3B*	*MAF*	*PIK3CA*	*SLC22A2*	*TIMP3*	*XRCC5*
ATP1A3	*CCL5*	*CSNK2A1*	*ERCC1*	*HTR3A*	*MAP2*	*PIK3CG*	*SLC22A3*	*TK1*	*YY1*
ATP1B1	*CCL7*	*CSNK2A2*	*ERCC2*	*HTR3B*	*MAP2K7*	*PMAIP1*	*SLC22A4*	*TK2*	*ZFPM2*
ATP1B2	*CCNA1*	*CSNK2B*	*ERCC3*	*HUS1*	*MAP4*	*PMP22*	*SLC22A5*	*TNFRSF10A*	*ZNF144*
ATP1B3	*CCNA2*	*CX3CL1*	*ERCC4*	*IFNB1*	*MAPK8*	*PMS1*	*SLC22A6*	*TNFRSF10B*	
ATP1B4	*CCND1*	*CX3CR1*	*ERCC5*	*IFNG*	*MAPK8IP2*	*PMS2*	*SLC22A7*	*TNFRSF11A*	
ATP7B	*CCND3*	*CXCL1*	*ERCC6*	*IGFBP3*	*MAPT*	*PNKP*	*SLC22A8*	*TNFRSF1A*	
ATR	*CCNE2*	*CXCL12*	*ESR1*	*IGSF6*	*MBD4*	*POR*	*SLC35A2*	*TNFRSF1B*	
ATRX	*CCNH*	*CXCL13*	*EXO1*	*IKBKB*	*MDM2*	*PPP1R15A*	*SLC38A1*	*TNFRSF6*	
BAD	*CCR1*	*CXCL14*	*FAF1*	*IL10*	*MGMT*	*PRKCA*	*SMC1L1*	*TNFRSF6B*	
BANF1	*CCR2*	*CXCL6*	*FANCA*	*IL11*	*MLH1*	*PRKCB1*	*SMC2L1*	*TNFSF10*	
BAX	*CCR5*	*CXCR3*	*FANCC*	*IL12A*	*MLH3*	*PRKCG*	*SMC4L1*	*TNFSF6*	
BCL2	*CCR6*	*CXCR4*	*FANCD2*	*IL12B*	*MNAT1*	*PRKCQ*	*SMPD2*	*TOP1*	
BID	*CCR7*	*CXCR6*	*FANCE*	*IL12RB1*	*MPG*	*PRKDC*	*SOD1*	*TOP2A*	
BIRC1	*CCR9*	*CYP17*	*FANCF*	*IL12RB2*	*MRE11A*	*PTGER2*	*SOD2*	*TOP2B*	
BIRC3	*CCRL1*	*CYP1B1*	*FANCG*	*IL13*	*MSH2*	*RAD17*	*SOD3*	*TOP3A*	

screening the loci, a Fisher's exact text for a 2 × 2 contingency table was done on all possible SNPs mapped to and around the loci, assuming allele frequency, dominant, or recessive models.

Estimation of probability of radiation dermatitis. The probability of radiation dermatitis was calculated for each combination of the two SNPs selected during the second-step screening process. To compute the probability, a logistic regression model with four indicator variables for the two different SNPs was adopted. The allele frequencies of each genotype combination were then calculated based on the allele frequency of individual SNPs obtained from our genotyping data of 1,594 unrelated Japanese individuals.

Results

Patient characteristics. The major patient characteristics and therapeutic variables are summarized in Table 2. About the patient-related factors, age, menopausal state, and the pathologic T and N classifications were similar in the radiation dermatitis and control groups. The two groups were generally well balanced with regard to the treatment-related factors such as the type of surgery, period between surgery and the commencement of radiotherapy, the presence of concurrent chemotherapy with oral fluorouracil, the radiation source, the total radiation dose to the whole breast, the dose per fraction, the overall treatment time for whole-breast radiation, and the accumulative dose per week. A significant difference was found for only one factor, the presence of concurrent tamoxifen chemotherapy; 51% of the radiation dermatitis group and 68% of the control group ($P = 0.024$) had received tamoxifen during the radiotherapy period.

Genotyping of SNPs. The genotypes of several loci were determined using an Invader assay in 156 patients with breast

cancer who received radiation therapy and 1,438 unrelated subjects. Consequently, the genotypes of 3,144 SNPs covering 494 genes were determined. The genes investigated in this study are listed in Table 1. To obtain accurate results in this case-control study, SNPs that departed from Hardy-Weinberg equilivbrium or that had a low minor allele frequency were excluded from further examination. Consequently, 2,651 SNPs were chosen for further analysis. The accuracy of the genotyping was tested by comparing the genotypes determined using the Invader assay with those determined using a RFLP analysis. More than 1,000 genotypes were assayed in three randomly chosen SNP loci. No genotypes showed any discrepancies between the two methods, indicating that the Invader assay had produced highly accurate genotypes (data not shown).

Identification of SNPs associated with radiation dermatitis. As a result of the screening steps described above, two loci were found to be associated with an adverse effect: the *IL12RB2* gene locus and the *ABCA1* gene locus. At the *IL12RB2* locus, 13 SNPs were examined (Supplementary Table S1). Among them, five SNPs were associated with radiation dermatitis (Table 3A). The strongest association was observed at SNP-K (rs3790568) in recessive model (P = 0.0065). To test the possibility that known coding SNPs mapped to the *IL12RB2* gene were associated with radiation dermatitis, we searched a dbSNP database and found six coding SNPs (rs2307146, rs7526769, rs2307148, rs2307145, rs2307153, and rs2307154). The genotypes of these coding SNPs were determined, but all the patients were wild-type (data not shown). At the *ABCA1* locus, 50 SNPs were analyzed (Supplementary Table S2); 8 SNPs were associated with radiation dermatitis, and the lowest P value of which was 0.0013 for SNP-17 (rs2253304) in allele frequency model (Table 3B). No other locus was associated with radiation dermatitis.

Haplotype block structure of* IL12RB2 *and* ABCA1 *gene loci. To narrow down the loci associated with radiation dermatitis, the haplotype block structures of both genes were estimated. The haplotypes and diplotypes of 13 SNPs at the *IL12RB2* locus were estimated in 1,594 unrelated individuals. Using the diplotypes of these individuals, the haplotype block structure of the *IL12RB2* locus was estimated using AdBlock software. Consequently, the 13 SNPs at the *IL12RB2* locus were subdivided into three haplotype blocks. All the SNPs associated with an adverse effect were located in the second haplotype block (Supplementary Table S1). As for the *ABCA1* gene, haplotype block analysis of the *ABCA1* gene revealed that the locus was subdivided into seven haplotype blocks. The SNPs

Table 2. Summary of patient characteristics and therapeutic variable

	Dermatitis group	Control group	P
Age (y)			
Median (range)	48 (30-73)	48 (23-77)	NS
Menopausal state			
Premenopausal	48	51	NS
Postmenopausal	29	28	
pT			
1	46	50	NS
2	31	28	
3	0	1	
pN			
0	58	67	NS
1	19	12	
Surgery			
Quadrantectomy	16	15	NS
Wide excision	61	64	
Surgery-radiotherapy interval (d)			
Median (range)	28 (10-123)	30 (3-233)	NS
Radiation source			
^{60}Co γ-rays	22	30	NS
4 MV X-rays	38	34	
6 MV X-rays	17	15	
Total radiation dose to whole breast (Gy)			
Median (range)	50 (44-52)	50 (44-52)	NS
Treatment time for whole-breast radiotherapy (d)			
Median (range)	36 (29-48)	36 (25-51)	NS
Dose per fraction (Gy)			
Median (range)	2.0 (1.8-2.2)	2.0 (1.8-2.2)	NS
Accumulative radiation dose per week (Gy/wk)			
Median (range)	9.6 (6.6-10.8)	9.6 (6.9-12.3)	NS
Concurrent tamoxifen			
Yes	39	54	0.024
No	38	25	
Concurrent oral fluorouracil			
Yes	25	32	NS
No	52	47	
Total	77	79	

Abbreviation: NS, not significant.

Table 3. Association between genes and radiation dermatitis

SNP name	Genotype	Dermatitis group	Control group	P	Odds ratio (95% CI)
A. Association between IL12RB2 and radiation dermatitis					
SNP-H (rs3790566)	CC	48	32	0.0065	2.45 (1.23-4.97)
	CT and TT	28	46		
SNP-I (rs379056)	GG	49	32	0.0062	2.50 (1.25-5.06)
	AG and AA	28	46		
SNP-K (rs3790568)	GG	51	34	0.0060	2.52 (1.26-5.13)
	AG and AA	26	44		
B. Association between ABCA1 and radiation dermatitis					
SNP-15 (rs2230806)	AA	13	29	0.0014	2.91 (1.30-6.78)
	AG and GG	63	48		
SNP-17 (rs2253304)	TT	13	29	0.0013	3.02 (1.35-7.04)
	CT and CC	64	47		
SNP-13 (rs2487058)	AA	13	28	0.0025	2.83 (1.26-6.67)
	AG and GG	61	46		

Abbreviation: 95% CI, 95% confidence interval.

associated with an adverse effect were located in the third and fifth haplotype blocks (Supplementary Table S2).

Estimation of the probability of radiation dermatitis for combined genotypes. To assess the probability of radiation dermatitis precisely, the genotypes of the two loci were used in a logistic regression model to estimate the probability of radiation dermatitis. Model selection using Akaike information criterion selected the best pair of SNPs, which consisted of SNP-15 in ABCA1 and SNP-K in IL12RB2. These analyses revealed that the genotype combination of a G homozygote at both SNP-15 and SNP-K exhibited the highest probability (0.75) of developing radiation-induced dermatitis (Table 4). This result indicates that 75% of patients carrying the combination of genotype have a chance to develop radiation-induced dermatitis. The genotype frequencies of these two SNPs were estimated based on genotyping data from 1,594 unrelated individuals. Based on these results, the frequency of the genotype with the highest probability of radiation dermatitis was estimated to be 0.147 in the Japanese population (Table 4).

Discussion

In this study, we showed associations between polymorphisms in the *IL12RB2* and *ABCA1* loci and an adverse effect in patients who received radiation therapy after undergoing surgery for breast cancer. SNPs associated with radiation dermatitis were observed in one or two of the haplotype blocks of the *IL12RB2* or *ABCA1* genes, respectively. These observations indicated that the associations between the SNPs and the adverse effect were nonrandom events.

Interleukin-12 (IL-12) receptor is a heterodimer protein consisting of two subunits: IL12RB1 and IL12RB2 (14). Several studies have shown that IL12RB2 may regulate IL-12 function (15). On the other hand, the cytokine IL-12 shows a wide variety of biological activities both *in vitro* and *in vivo*. Several studies have shown the antitumor activity of IL-12 through an effect on the host immune system. Schwarz et al. (16) reported that IL-12 suppresses UV radiation-induced apoptosis. IL-12 also prevents immunosuppression caused by UV irradiation. They concluded that IL-12 induces the expression of genes involved in nucleotide excision repair and that the activated nucleotide excision repair system may protect UV-irradiated cells from undergoing apoptosis. In their report, IL-12 was unable to suppress apoptosis caused by γ-irradiation *in vitro*. However, the effect of IL-12 on γ-irradiated cells *in vivo* remains to be observed. Our results may suggest that changes in the genotype of SNPs in IL12RB2 may regulate the biological function of IL-12, causing differences in the biological response to ionizing radiation.

The association between radiation-induced dermatitis and polymorphisms in the *ABCA1* gene is rather unexpected because the *ABCA1* gene plays an essential role in the efflux of cholesterol to high-density lipoprotein. However, the *ABCA1* gene has also been shown to be involved in the engulfment of apoptotic cells. Hamon et al. (17) showed that the loss of ABCA1 function impaired the engulfment of cell corpses generated by apoptosis. This result also suggests that the functions of the ABCA1 gene product are linked to apoptosis. In our study, a coding SNP (SNP-15; rs2230806), in which the nucleotide polymorphisms cause an amino acid substitution from Lys to Arg at the 219th amino acid, was associated with radiation-induced dermatitis. Considering the link between the *ABCA1* gene and apoptosis, this amino acid substitution may influence apoptotic reactions caused by ionizing radiation, thereby influencing the degree of dermatitis that occurs.

Table 4. Probability of radiation dermatitis for each genotype

rs2230806 (ABCA1)	rs3790568 (IL12RB2)	
	GG	AG or AA
GG	0.75 (0.147)	0.527 (0.093)
AG or AA	0.558 (0.466)	0.314 (0.294)

NOTE: Numbers in parentheses indicate genotype frequency in the Japanese population.

Data interpretation. The patient selection policy of the present study was developed to minimize the problems that a multi-institutional case-control study is liable to suffer. This policy was characterized by the patient-to-patient matching selection to avoid intergroup bias, the photograph-based confirmation for grading dermatitis, and the dose distribution-based exclusion of radiotherapy-related confounding factors.

In spite of patient-to-patient matching for the major prognostic factors, the proportion of patients treated with concurrent tamoxifen therapy were significantly larger in the control group than in the radiation dermatitis group ($P = 0.024$). This difference was the only intergroup bias observed out of all the patient- and treatment-related factors. The clinical significance of concurrent tamoxifen therapy in radiotherapy-related toxicity is controversial. Several reports have shown an increased risk of pulmonary and breast fibrosis after concurrent treatment with tamoxifen therapy and radiotherapy (18, 19), whereas other reports did not show any risk (20). Furthermore, an *in vitro* experimental study showed that the radiosensitivity of hormone-dependent breast cancer cells might be reduced through the cytostatic effect of tamoxifen (21). However, no experimental or clinical studies have suggested a radioprotective effect of tamoxifen on hormone-independent normal cells, including lymphocytes or fibroblasts. Therefore, we suspect that this intergroup bias did not seriously affect the interpretation of the SNP data.

Clinical relevance. Many *ex vivo* prediction systems have been developed and evaluated in which various numbers of patients treated with radiotherapy were studied prospectively or retrospectively using cellular or molecular *ex vivo* assays of lymphocytes or fibroblasts, with acute or late adverse effects as the clinical end points. The results of studies comparing clinical and cellular radiosensitivity using colony assays, micronucleus assays, and comet assays were often suggested to be promising. However, as reviewed by Twardella and Chang-Claude (22), the clinical relevance of these predictive assays should be carefully evaluated, considering any possible bias that may arise from inappropriate settings of patient cohorts, poorly defined clinical end points, or contamination by confounding external factors.

Recently, several studies have been undertaken to evaluate the correlation between clinical radiosensitivity and SNPs (23–26). Mostly, SNPs in selected genes whose functions may modify radiation-related toxicity, such as *ATM*, *TGFB1*, and *XRCC1*, have been analyzed. For instance, Andreassen et al. (23) analyzed seven SNPs in five genes (*TGFB1*, *SOD2*, *XRCC1*, *XRCC3*, and *APEX*) using cultured fibroblasts obtained from 41 patients who had been treated with uniform postmastectomy radiotherapy. Their data indicated that five of the seven SNPs were significantly correlated with the occurrence of grade 3 s.c. fibrosis or grade 2 to 3 telangiectasia in the irradiated skin. They concluded that SNP analysis may have the potential to predict clinical radiosensitivity, particularly when multiple SNPs are analyzed.

By logistic regression analysis, probabilities of radiation-induced dermatitis were estimated on each combination of genotypes of two SNPs (rs3790568 and rs2230806). These analyses revealed that three patients in four patients carrying a specific combination of genotypes, G homozygote in two SNPs, develop radiation-induced dermatitis. Genotype frequency of combination of the SNPs was estimated as 0.147 in the Japanese population. Therefore, ~11% of Japanese are predicted to develop radiation-induced dermatitis. Considering incidence of radiation-induced dermatitis (5-10%), this number seems to be reasonable.

The present study featured a much more comprehensive SNP analysis than any other previous study. At least a considerable part of clinically observed hyperradiosensitivity may be regulated by the integration of multiple minor alterations in genetic function. Therefore, a comprehensive analysis, as was done in the present study, is most suitable for identifying radiosensitive populations of patients. These results may serve as preliminary data for the construction of personalized radiation therapy.

Disclosure of Potential Conflicts of Interest

No potential conflicts of interest were disclosed.

Acknowledgments

We thank the patients for participating in the study and Yusaku Wada, Yuko Kanto, and Kiyoko Ogawa for their technical assistance.

References

1. Hiraoka M, Mitsumori M, Kokubo M. The roles and controversies of radiation therapy in breast conserving therapy for breast cancer. Breast Cancer 1997;4:127–33.
2. Rosen EM, Fan S, Rockwell S, Goldberg ID. The molecular and cellular basis of radiosensitivity: implications for understanding how normal tissues and tumors respond to therapeutic radiation. Cancer Invest 1999;17:56–72.
3. Fujishiro S, Mitsumori M, Kokubo M, et al. Cosmetic results and complications after breast conserving therapy for early breast cancer. Breast Cancer 2000; 7:57–63.
4. Morgan JL, Holcomb TM, Morrissey RW. Radiation reaction in ataxia telangiectasia. Am J Dis Child 1968; 116:557–8.
5. Gotoff SP, Amirmokri E, Liebner EJ. Ataxia telangiectasia. Neoplasia, untoward response to x-irradiation, and tuberous sclerosis. Am J Dis Child 1967;114: 617–25.
6. Alter BP. Radiosensitivity in Fanconi's anemia patients. Radiother Oncol 2002;62:345–7.
7. Burnet NG, Peacock JH. Normal cellular radiosensitivity in an adult Fanconi anaemia patient with marked clinical radiosensitivity. Radiother Oncol 2002;62: 350–1; author reply 1–2.
8. Distel L, Neubauer S, Varon R, Holter W, Grabenbauer G. Fatal toxicity following radio- and chemotherapy of medulloblastoma in a child with unrecognized Nijmegen breakage syndrome. Med Pediatr Oncol 2003;41: 44–8.
9. Tauchi H, Matsuura S, Kobayashi J, Sakamoto S, Komatsu K. Nijmegen breakage syndrome gene, NBS1, and molecular links to factors for genome stability. Oncogene 2002;21:8967–80.
10. Turesson I, Nyman J, Holmberg E, Oden A. Prognostic factors for acute and late skin reactions in radiotherapy patients. Int J Radiat Oncol Biol Phys 1996;36: 1065–75.
11. Hirakawa M, Tanaka T, Hashimoto Y, et al. JSNP: a database of common gene variations in the Japanese population. Nucleic Acids Res 2002;30:158–62.
12. Haga H, Yamada R, Ohnishi Y, Nakamura Y, Tanaka T. Gene-based SNP discovery as part of the Japanese Millennium Genome Project: identification of 190,562 genetic variations in the human genome. Single-nucleotide polymorphism. J Hum Genet 2002;47: 605–10.
13. Fujisawa H, Eguchi S, Ushijima M, et al. Genotyping of single nucleotide polymorphism using model-based clustering. Bioinformatics 2004;20:718–26.
14. Presky DH, Yang H, Minetti LJ, et al. A functional interleukin 12 receptor complex is composed of two β-type cytokine receptor subunits. Proc Natl Acad Sci U S A 1996;93:14002–7.
15. Rogge L, Barberis-Maino L, Biffi M, et al. Selective expression of an interleukin-12 receptor component by human T helper 1 cells. J Exp Med 1997;185: 825–31.
16. Schwarz A, Stander S, Berneburg M, et al. Interleu-

kin-12 suppresses ultraviolet radiation-induced apoptosis by inducing DNA repair. Nat Cell Biol 2002;4:26–31.

17. Hamon Y, Chambenoit O, Chimini G. ABCA1 and the engulfment of apoptotic cells. Biochim Biophys Acta 2002;1585:64–71.
18. Huang EY, Wang CJ, Chen HC, et al. Multivariate analysis of pulmonary fibrosis after electron beam irradiation for postmastectomy chest wall and regional lymphatics: evidence for non-dosimetric factors. Radiother Oncol 2000;57:91–6.
19. Bentzen SM, Skoczylas JZ, Overgaard M, Overgaard J. Radiotherapy-related lung fibrosis enhanced by tamoxifen. J Natl Cancer Inst 1996;88:918–22.
20. Pierce LJ, Hutchins LF, Green SR, et al. Sequencing of tamoxifen and radiotherapy after breast-conserving surgery in early-stage breast cancer. J Clin Oncol 2005;23:24–9.
21. Wazer DE, Tercilla OF, Lin PS, Schmidt-Ullrich R. Modulation in the radiosensitivity of MCF-7 human breast carcinoma cells by 17B-estradiol and tamoxifen. Br J Radiol 1989;62:1079–83.
22. Twardella D, Chang-Claude J. Studies on radiosensitivity from an epidemiological point of view—overview of methods and results. Radiother Oncol 2002;62:249–60.
23. Andreassen CN, Alsner J, Overgaard M, Overgaard J. Prediction of normal tissue radiosensitivity from polymorphisms in candidate genes. Radiother Oncol 2003;69:127–35.
24. Angele S, Romestaing P, Moullan N, et al. ATM haplotypes and cellular response to DNA damage: association with breast cancer risk and clinical radiosensitivity. Cancer Res 2003;63:8717–25.
25. Severin DM, Leong T, Cassidy B, et al. Novel DNA sequence variants in the hHR21 DNA repair gene in radiosensitive cancer patients. Int J Radiat Oncol Biol Phys 2001;50:1323–31.
26. Fernet M, Hall J. Genetic biomarkers of therapeutic radiation sensitivity. DNA Repair (Amst) 2004;3:1237–43.

Int. J. Radiation Oncology Biol. Phys., Vol. 70, No. 2, pp. 626–633, 2008

0360-3016/08/$–see front matter

ELSEVIER

doi:10.1016/j.ijrobp.2007.09.053

PHYSICS CONTRIBUTION

IN VIVO DOSIMETRY OF HIGH-DOSE-RATE INTERSTITIAL BRACHYTHERAPY IN THE PELVIC REGION: USE OF A RADIOPHOTOLUMINESCENCE GLASS DOSIMETER FOR MEASUREMENT OF 1004 POINTS IN 66 PATIENTS WITH PELVIC MALIGNANCY

TAKAYUKI NOSE, M.D.,*† MASAHIKO KOIZUMI, M.D.,‡ KEN YOSHIDA, M.D.,§ KINJI NISHIYAMA, M.D.,‡ JUNICHI SASAKI,‡ TAKESHI OHNISHI,‡ TAKUYO KOZUKA, M.D.,* KOTARO GOMI, M.D.,* MASAHIKO OGUCHI, M.D.,* IORI SUMIDA, PH.D.,*† YUTAKA TAKAHASHI, PH.D.,† AKIRA ITO, PH.D.,† AND TAKASHI YAMASHITA, M.D.*†

*Department of Radiation Oncology, The Cancer Institute Hospital of the Japanese Foundation for Cancer Research, Tokyo, Japan; †Department of Physics, The Cancer Institute of the Japanese Foundation for Cancer Research, Tokyo, Japan; ‡Department of Radiation Oncology, Osaka Medical Center, Osaka, Japan; and §Department of Radiology, Osaka National Hospital, Osaka, Japan

Purpose: To perform the largest *in vivo* dosimetry study for interstitial brachytherapy yet to be undertaken using a new radiophotoluminescence glass dosimeter (RPLGD) in patients with pelvic malignancy and to study the limits of contemporary planning software based on the results.

Patients and Methods: Sixty-six patients with pelvic malignancy were treated with high-dose-rate interstitial brachytherapy, including prostate (n = 26), gynecological (n = 35), and miscellaneous (n = 5). Doses for a total of 1004 points were measured by RPLGDs and calculated with planning software in the following locations: rectum (n = 549), urethra (n = 415), vagina (n = 25), and perineum (n = 15). Compatibility (measured dose/calculated dose) was analyzed according to dosimeter location.

Results: The compatibility for all dosimeters was 0.98 ± 0.23, stratified by location: rectum, 0.99 ± 0.20; urethra, 0.96 ± 0.26; vagina, 0.91 ± 0.08; and perineum, 1.25 ± 0.32.

Conclusions: Deviations between measured and calculated doses for the rectum and urethra were greater than 20%, which is attributable to the independent movements of these organs and the applicators. Missing corrections for inhomogeneity are responsible for the 9% negative shift near the vaginal cylinder (specific gravity = 1.24), whereas neglect of transit dose contributes to the 25% positive shift in the perineal dose. Dose deviation of >20% for nontarget organs should be taken into account in the planning process. Further development of planning software and a real-time dosimetry system are necessary to use the current findings and to achieve adaptive dose delivery.

Radiotherapy, *In vivo* dosimetry, Radiophotoluminescence glass dosimeter, Brachytherapy, High dose rate.

INTRODUCTION

Contemporary planning software for high-dose-rate (HDR) brachytherapy enables radiation oncology teams to determine conformal dose distribution to the target while avoiding excessive doses to critical organs (1–4); however, reproducibility of planned doses in interstitial brachytherapy has not been well recognized. Few studies have investigated *in vivo* dosimetry for interstitial brachytherapy; previous studies have dealt with small numbers of patients (≤10 patients, to the best of our knowledge) and have been limited to the use of thermoluminescence dosimeters (TLD), the use of which involves complex handling processes (5–9).

A radiophotoluminescence glass dosimeter (RPLGD) was developed in the 1950s and has subsequently been used for radiotherapeutic dosimetry at a small number of centers (10–14). Irradiation of silver-activated phosphate glass converts silver ions to stable luminescent centers; when exposed to ultraviolet light, the luminescent centers produce fluorescence in proportion to the absorbed radiation dose. RPLGDs possess ideal properties for *in vivo* dosimetry, including small

Reprint requests to: Takayuki Nose, M.D., Department of Radiation Oncology, The Cancer Institute Hospital of the Japanese Foundation for Cancer Research, 3-10-6 Ariake, Koto-Ku, Tokyo 135-8550, Japan. Tel: (+81) 3-3520-0111; Fax: (+81) 3 3570 0343; E-mail: takayuki.nose@jfcr.or.jp

Conflict of interest: none.

Acknowledgments—The authors are grateful to Dr. Teizou Tomaru (Chiyoda Technol) and Mr. Tatsuya Ishikawa (Asahi Techno Glass) for their valued advice concerning radiation physics. This study was supported in part by a Grant-in-Aid for Scientific Research (C) from the Japan Society for the Promotion of Science (18591397). This study was presented at the 12th International Brachytherapy Conference, June 20–23, 2007, in Rome, Italy.

Received March 3, 2007, and in revised form Sept 19, 2007. Accepted for publication Sept 21, 2007.

size, ruggedness, nontoxicity, photon-energy independence over the energy range >0.2–0.3 MeV, high sensitivity, good reproducibility, and repeat readability until annealing of the detectors. Advances in technology (10–15) have helped to overcome initial shortcomings in the method, such as energy dependence in the low-energy range of <0.1 MeV, susceptibility to spurious readings with surface contamination, and the necessity for complex handling and cleaning processes. Newly developed RPLGDs (Dose Ace, Chiyoda Technol, Tokyo, Japan) were used in the current study (10–12). In our previous study, using RPLGD, we performed the largest *in vivo* dosimetry study examined at that time by measuring 83 points in 61 head and neck cancer patients (12). In the current study, we investigate the reproducibility of pelvic interstitial brachytherapy by measuring 1004 points in 66 pelvic malignancy patients. On the basis of the results, we investigated the limits of available planning software and a potential solution for precise dose delivery.

PATIENTS AND METHODS

Patients

Sixty-six patients with pelvic malignancy underwent HDR interstitial brachytherapy (HDRIB) with RPLGD at Osaka Medical Center (OMC) between 2000 and 2003. Patient characteristics are presented in Table 1. The median follow-up period was 30 months (range, 1–58 months). Forty-three patients displayed nonrecurrent disease, and 23 patients displayed recurrent disease following surgery ($n = 11$), radiation ($n = 4$), or both ($n = 8$). All patients were informed of the study purposes and possible consequences. Written informed consent was obtained before participation.

Radiophotoluminescence glass dosimeter

The RPLGD (Dose Ace) is more robust than TLDs and is composed of uniform glass with an effective atomic number of 12.039; it contains 11.00% Na, 31.55% P, 51.16% O, 6.12% Al, and 0.17% Ag by weight (10). The element is 1.5 mm in diameter and 8.5 mm in length, which is similar to commercially available TLD rods. The sensitive volume is located centrally and measures 1.5 mm in diameter and 6.0 mm in length; a portion 1.5 mm in diameter and 1.25 mm in length at each end is not used for dosimetry. The dispersion of response among dosimeters is small (coefficient of variation [ratio of the standard deviation to the mean] = 0.82%), and the reproducibility of repeat measurements by a single element is excellent (coefficient of variation = 0.29%), being superior to that of commercially available TLDs (10). Moreover, handling of the RPLGD is easier than for TLDs. A reader (FGD-1000, Chiyoda Technol, Tokyo, Japan) stimulates the RPLGD using a pulsed ultraviolet laser. Differences in fluorescence decay time between surface contamination (0.3 μs) and radiophotoluminescence (3 μs) enable discrimination between signal arising from contamination with finger grease or mucus from that due to absorbed radiation dose (10, 15, 16); thus, the new detector can be easily inserted and removed manually into and out of vectors and can be applied to regions in close contact with mucus because it does not require the complex cleaning processes necessary for TLDs and early RPLGDs. The reader repeats measurements 10–50 times within a few seconds and averages the values to reduce random errors. The quantity of radiophotoluminescence of a RPLGD is compared with that of a standard detector within the reader that has been irradiated with a known dose; the readout is expressed in Gy. Readout range is 10 μGy to 10 Gy, extendable to 500 Gy with optional settings. These new capabilities, coupled with the inherent properties of RPLGDs, mean that the new dosimeter can be easily applied to *in vivo* dosimetry studies. A preheat process at 70°C for 30 min and a cooling process to room temperature are necessary before each reading for which immediate reading after irradiation cannot be achieved. The details of individual correction factors derived using 4 MV X-rays have previously been described (12). For the 100 RPLGDs used in the current study, the coefficient of variation was 1.41% for dispersion among detectors, and the mean coefficient of variation for three-time repeat measurement was 1.29%. The linear dose response for RPLGD ($r = 1.000$, $p < 0.01$) for 1 to 136 Gy has been confirmed in our previous study (12).

Table 1. Patient characteristics

Age	Median 64 (35–81)
Sex	Male 30, female 36
Follow-up	Median 30 (1~58) months
Primary site	
Prostate	26
Gynecological	35 (previously irradiated 11)
Miscellaneous	5 (previously irradiated 1)
Total	66

RPLGD Vectors

Three types of vectors were developed for this study. Type 1 is a single "RPLGD complex", which was loaded to a 1.5-mm-deep slot carved on the upper part of the vaginal cylinder or on the perineal side of the template and was covered with gum paint (Fig. 1a); the RPLGD was located centrally, with a ø1-mm lead ball placed at each end as a radio-opaque marker. A 1-mm-long urethane spacer was placed between the RPLGD and each lead ball to avoid scratching. The Type 2 vector, used for the urethra, comprised a train of 10 "RPLGD complexes" loaded in a ø2-mm Teflon tube (Figs. 1b and 1c). The Type 3 vector, dedicated to the rectum, used a ø4-mm Teflon tube into which a train of 10 "encapsulated RPLGD complexes" was loaded manually; each RPLGD was contained in a plastic capsule to avoid excessive contamination by mucus (Fig. 1d). Three nylon threads were sutured to each end and to the midportion of the vector for fixation to the rectum.

Implantation

Implantation was performed in a lithotomy position under general and epidural anesthesia with or without spinal anesthesia. Before implantation, the Type 3 vector was sutured to the anterior rectal wall through a rigid rectoscope (Figs. 2a, 2b, and 2c). The entire vector length was kept in contact with the mucosa using at least three stitches; additional sutures were used if the vector was not in full contact with the mucosa. A median of 18 metal needles (range, 5–29) were implanted using a perineal template. Implant geometry was preplanned to cover the clinical target volume (CTV) with 85% basal dose isodose surface (BDIS) following the extrapolated Paris System to more than two-plane implants (17). Needle placement was guided by palpation and transrectal/vaginal ultrasound. For female patients, the vaginal cylinder was attached perpendicular to the template (Figs. 2a and 2b). The vaginal cylinder and metal needles were fixed to the template using screws and a template cap such that they were unified as a group and could only move

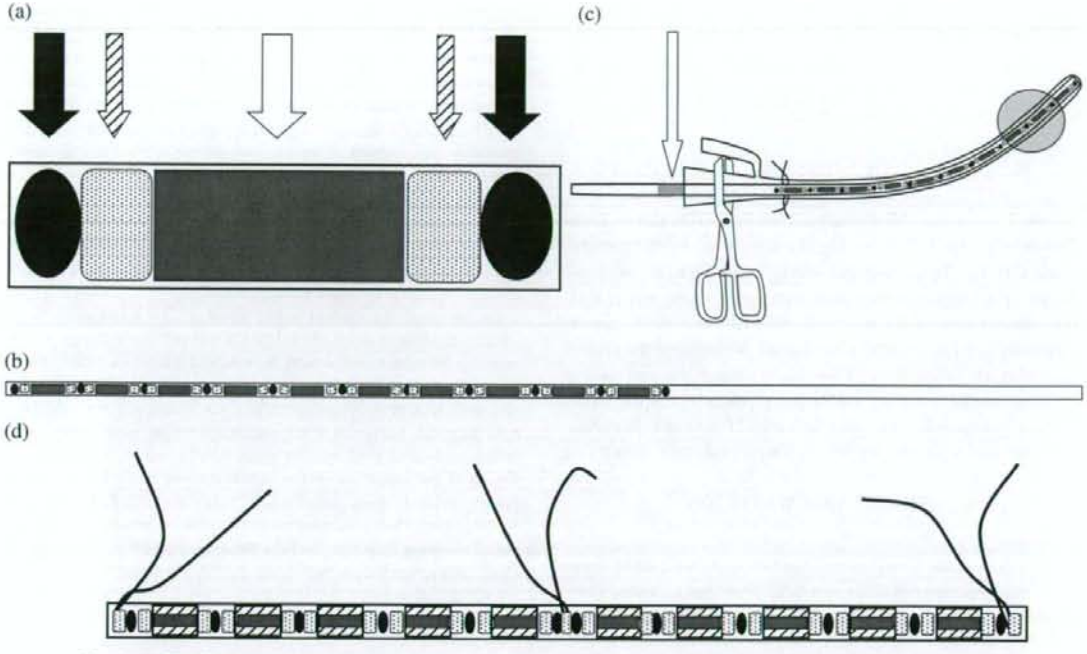

Fig. 1. (a) The Type 1 vector consists of a 1.5–mm-deep slot, carved on a vaginal cylinder or on a template; this houses an radiophotoluminescence glass dosimeter (RPLGD) complex, which consists of an RPLGD (white arrow) located centrally, a ø1 mm lead ball (black arrows) placed at each end, and 1-mm spacers (striped arrows) between the RPLGD and the lead balls. (b) The Type 2 vector, dedicated to the urethra; the ø2 mm Teflon tube contains 10 RPLGD complexes. (c) The Type 2 vector is inserted into the balloon catheter until the vector top touches the proximal catheter end at simulation and at each irradiation session. The vector and the catheter are clamped together with forceps near the distal catheter end. The point where the vector surface crosses the distal end of the catheter is marked using a felt-tip pen (arrow). (d) The Type 3 vector, dedicated to the rectum, is shown; the ø4-mm Teflon tube contains 10 encapsulated RPLGD complexes, with each RPLGD housed in a plastic capsule. The three nylon threads sutured to each end and the midportion of the vector enable fixation of the vector to the rectum.

synchronously. For most female patients, tumor extent involved the vaginal wall such that vaginal wall dosimetry represented tumor dose. The template was sutured to the perineum such that the Type 1 RPLGD was in contact with the skin (Figs. 2a and 2b). Template dosimetry represented perineal skin dose. A balloon catheter was sutured to the urethral orifice after early experiences with the prostate implant and anterior vaginal implant in particular; the needle tips had collapsed the balloon and caused migration of the catheter from the original position. A total of 1142 points were measured by RPLGDs in the following locations: anterior wall of the rectum, $n = 599$; urethra, $n = 482$; vaginal cylinder, $n = 28$; perineal template, $n = 33$. Doses were measured by RPLGDs and were also calculated on a planning computer (CadplanBT 1.1, Varian TEM, Crawley, United Kingdom). Of the 1142 points, 58 points (5.1%) were not identified by X-ray films, and dose calculation was not obtainable; therefore, both measured and calculated doses were available for 1084 points.

Simulation, planning, and irradiation

At simulation, the Type 2 vector was inserted into the balloon catheter until the vector top touched the proximal end of the catheter (Fig. 1c). Both the vector and the catheter were clamped together with forceps near the distal end of the catheter. The point where the vector surface crossed the distal end of the catheter was marked with a felt-tip pen to enable reproducible loading at each session. A dummy source was loaded into each applicator. A pair of radiographs was taken; the couch was then rotated 90°, and CT was performed at 5-mm intervals; all measured doses were therefore contaminated by simulation radiation. CadplanBT 1.1 was used for treatment planning. The geometry of the applicators was reconstructed from the radiographs before the superimposition of CT data. The central plane and basal dose points were determined according to the extrapolated Paris System (17, 18). An arbitrary isodose surface (median, 82% BDIS; range, 70%–98% BDIS) that covered the CTV was chosen for dose prescription. HDRIB schedules are described in Table 2; rectal and urethral doses represent constraints for dose prescription. For patients not previously irradiated, calculated rectal and urethral doses were set to a below-ceiling dose that was determined on the basis of clinical experiences of HDRIB at Osaka University and related hospitals (Table 2). For the 12 reirradiated patients, the previous radiotherapy consisted of 30-Gy whole pelvis (range, 0–50 Gy) and 10-Gy central-shielded field (range, 0–28 Gy) combined with 30-Gy HDR intracavitary brachytherapy ($n = 6$, range, 15–30 Gy) or 36 Gy HDRIB ($n = 1$). It was impractical to set a ceiling dose for these patients, and doses for

the rectum/urethra were modified to as low as possible. The maximum diameter of double the prescription isodose surface (hyperdose sleeve) was another concern related to morbidity. The Paris System recommends keeping this diameter ≤8–10 mm (18). If the diameter exceeded 8 mm, the dose distribution was modified by manually changing dwell times. When these three conditions (CTV coverage, rectal/urethral dose, hyperdose sleeve ≤8 mm) could not be achieved simultaneously, the plan was compromised at the cost of rectal/urethral dose, hyperdose sleeve, or both. For each RPLGD, three points (the midpoint and both ends of the readout part) were reconstructed. Doses were calculated for the three points, and the averaged value was regarded as the calculated dose for the particular RPLGD. The anatomic location of the RPLGD was classified as "anterior wall of the rectum"; "urethra (male/female)"; "vaginal wall," measured at the vaginal cylinder surface; and "perineal skin," measured at the template surface facing the perineum. Irradiation was performed using Varisource (Varian TEM). Source strength was determined following each purchase using a well-type chamber. The mean deviation from the supplier's value was only 0.08 ± 0.83% (range, –1.04 to 1.60%). HDRIB was delivered twice a day with an interval of at least 6 h. Before each session, the Type 2 vector was inserted into the balloon catheter to the depth of the felt-tip pen marker crossing the catheter (Fig. 1c).

(a)

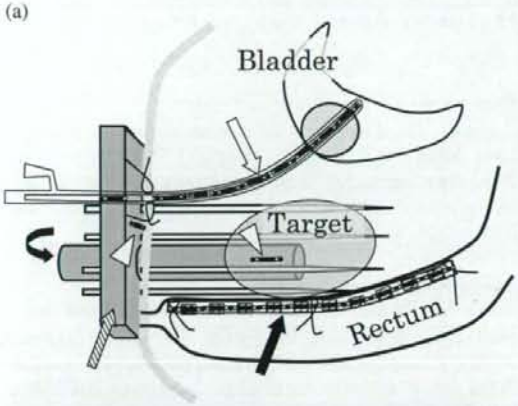

(b)

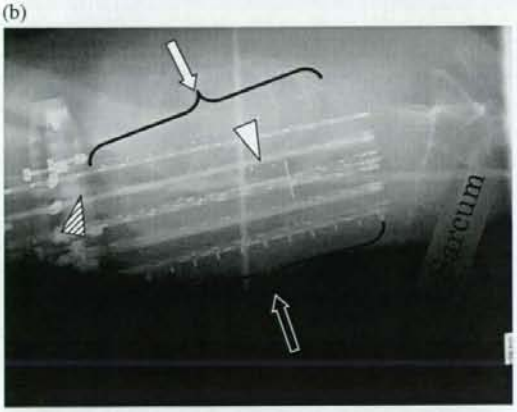

(c)

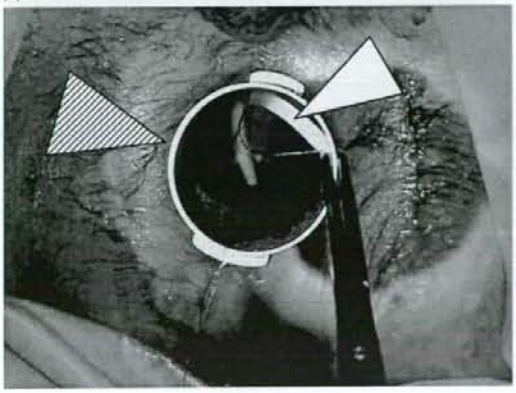

Absorbed simulation X-ray

Absorbed dose from the simulation was assessed in one prostate cancer patient using a Type 2 vector in the urethra. During a routine simulation, 10 RPLGDs in the urethra were exposed to 120 KV X-rays (mean effective energy ≈40 KeV) for a pair of radiographs and a 20-cm CT at 5-mm intervals. The readout value was corrected by both calibration factors for each RPLGD, as obtained for 4-MV photons, and by a relative correction factor of 3.8 for 40 KeV (Fig. A, 9.4 in ref. 16).

Statistics

Statistical analyses were performed using SPSS 8.0 software (Chicago, IL). The Mann-Whitney *U* test was used for nonparametric comparisons (19). Kaplan-Meier methods were used for analyses of local control (20).

RESULTS

Clinical results

There were no unexpected events attributable to the use of RPLGDs. Moreover, the location of anterior rectal wall that is not visible on CT was easily found, and the corresponding dose was calculated. In all patients, the use of RPLGD was well tolerated. The local control ratio was 87% with a median follow-up of 30 months. Late sequelae were graded as G0 in 38 patients, G1 in 6 patients, G2 in 5 patients, G3 in 7 patients, and not specified in 10 patients.

Fig. 2. (a) Schema of the current study. Application of two Type 1 radiophotoluminescence glass dosimeter (RPLGD) complexes: one on the template, the other on the vaginal cylinder (arrowheads); one Type 2 vector in a balloon catheter (white arrow); and one Type 3 vector on the anterior rectal wall (black arrow) for a female patient. The striped arrow indicates the perineal template and vaginal cylinder (curved arrow). (b) A radiograph from the study shows the application positions of the following vectors: Type 1 vectors on the template (striped arrowhead) and on the vaginal cylinder (white arrowhead); Type 2 vector in a balloon catheter (white arrow); and Type 3 vector on the anterior rectal wall (black arrow) of a female patient. (c) A Type 3 vector (white arrowhead) is sutured to the anterior rectal wall through a rigid rectoscope (striped arrowhead).

Table 2. HDRIB schedule

	HDRIB	EXRT	Ceiling dose for rectum	Ceiling dose for urethra
HDRIB alone (n = 45)				
Previously nonirradiated (n = 33)	54 Gy/9 fr/5 d	-	42 Gy/9 fr/5 d	76 Gy/9 fr/5 d
Previously irradiated (n = 12)	48 Gy/8 fr/4 d	-	Not specified	Not specified
HDRIB+EXRT (n = 21)				
Previously nonirradiated (n = 21)	30 Gy/5 fr/3 d	WP 30 Gy + CS 20 Gy	24 Gy/5fr/3 d	58 Gy/5 fr/3 d

Abbreviations: HDRIB = high-dose-rate interstitial brachytherapy; EXRT = external radiotherapy; fr = fraction; WP = whole pelvis field; CS = central-shielded field.

Absorbed simulation X-ray by RPLGDs

The median measured dose of all 1084 points was 17.19 Gy (range, 0.41–88.73 Gy). The median absorbed simulation dose for the 10 RPLGDs was 0.048 Gy (range, 0.043–0.054 Gy), corresponding to 1.06% (0.048 Gy × 3.8 / 17.19 Gy; range, 0.21% [0.048 Gy × 3.8 / 88.73 Gy] to 44.49% [0.048 Gy × 3.8 / 0.41 Gy]) of the median absorbed dose. Setting the threshold for the simulation dose at 5% of the total absorbed dose, 3.65 Gy (0.048 Gy × 3.8 / 5%) was the minimum total measured dose required. Doses for 80 points (rectum, n = 30; urethra, n = 41; vagina, n = 1; perineum, n = 8) were <3.65 Gy; these values were eliminated from further analyses.

Results of 1004 RPLGDs

The remaining 1004 points (≥3.65 Gy), comprised of rectum, n = 549; urethra, n = 415; vaginal wall, n = 25; and perineal skin, n = 15 were used for further analyses. For the 1004 dosimeters, the median measured and calculated doses were 18.59 Gy (range, 3.65–88.73 Gy) and 19.94 Gy (range, 2.42–94.68 Gy), respectively. The compatibility ratio of the measured and calculated doses was 0.98 ± 0.23. Measured doses, calculated doses, and compatibility according to location are displayed in Table 3. The frequencies of compatibility according to location are displayed in Figs. 5a–5e.

Dose for the rectum

For the 549 dosimeters, the median measured and calculated doses were 17.64 Gy (range, 3.68–64.64 Gy) and 18.32 Gy (range, 3.19–75.70 Gy), respectively. The compatibility ratio of the measured and calculated doses was 0.99 ± 0.20 (Fig. 3a).

Dose for the urethra (female and male)

For the 415 dosimeters, the median measured and calculated doses were 20.47 Gy (range, 3.72–88.73 Gy) and 21.65 Gy (range, 2.58–78.84 Gy), respectively. The compatibility ratio of the measured and calculated doses was 0.96 ± 0.26.

Dose for the male urethra

For the 181 dosimeters, the median measured and calculated doses were 28.31 Gy (range, 4.07–88.73 Gy) and 36.73 Gy (range, 3.35–78.84 Gy), respectively. The compatibility ratio of the measured and calculated doses was 0.90 ± 0.30 (Fig. 3b). The ratio for the male urethra was significantly different from that for the female urethra (p <0.01). Even with stitches to the urethral orifice in males, if the balloon was ruptured by the needle tips, the balloon catheter could migrate, depending on penis direction and length. A 10% negative shifted distribution suggests slipping of the original position.

Dose for the female urethra

For the 234 dosimeters, the median measured and calculated doses were 17.51 Gy (range, 3.72–71.69 Gy) and 18.16 Gy (range, 2.58–73.03 Gy), respectively. The compatibility ratio of the measured and calculated doses was 1.01 ± 0.20 (Fig. 3c).

Dose for the vaginal wall

For the 25 dosimeters, the median measured and calculated doses were 38.79 Gy (range, 9.51–82.42 Gy) and 42.98 Gy (range, 9.04–94.68 Gy), respectively. The compatibility ratio of the measured and calculated doses was 0.91 ± 0.08 (Fig. 3d).

Table 3. Measured dose, calculated dose, and compatibility according to locations for the 1004 points

Region	Measured dose	Calculated dose	Compatibility ratio*
Anterior wall of the rectum (n = 549)	17.6 Gy (3.7–64.6 Gy)	18.3 Gy (3.2–75.7 Gy)	0.99 ± 0.20
Urethra (n = 415)	20.5 Gy (3.7 Gy-88.7 Gy)	21.7 Gy (2.6 Gy-78.8 Gy)	0.96 ± 0.26
Male urethra (n = 181)	28.3 Gy (4.1 Gy-88.7 Gy)	36.7 Gy (3.4 Gy-78.8 Gy)	0.90 ± 0.30
Female urethra (n = 234)	17.5 Gy (3.7 Gy-71.7 Gy)	18.2 Gy (2.6–73.0 Gy)	1.01 ± 0.20
Vaginal wall (n = 25)	38.8 Gy (9.5 Gy-82.4 Gy)	43.0 Gy (9.0–94.7 Gy)	0.91 ± 0.08
Perineal skin (n = 15)	6.9 Gy (3.7 Gy-59.6 Gy)	6.3 Gy (2.4–61.6 Gy)	1.25 ± 0.32
Total (n = 1004)	18.6 Gy (3.7 Gy-88.7Gy)	19.9 Gy (2.4–94.7 Gy)	0.98 ± 0.23

* Compatibility ratio = measured dose/calculated dose.

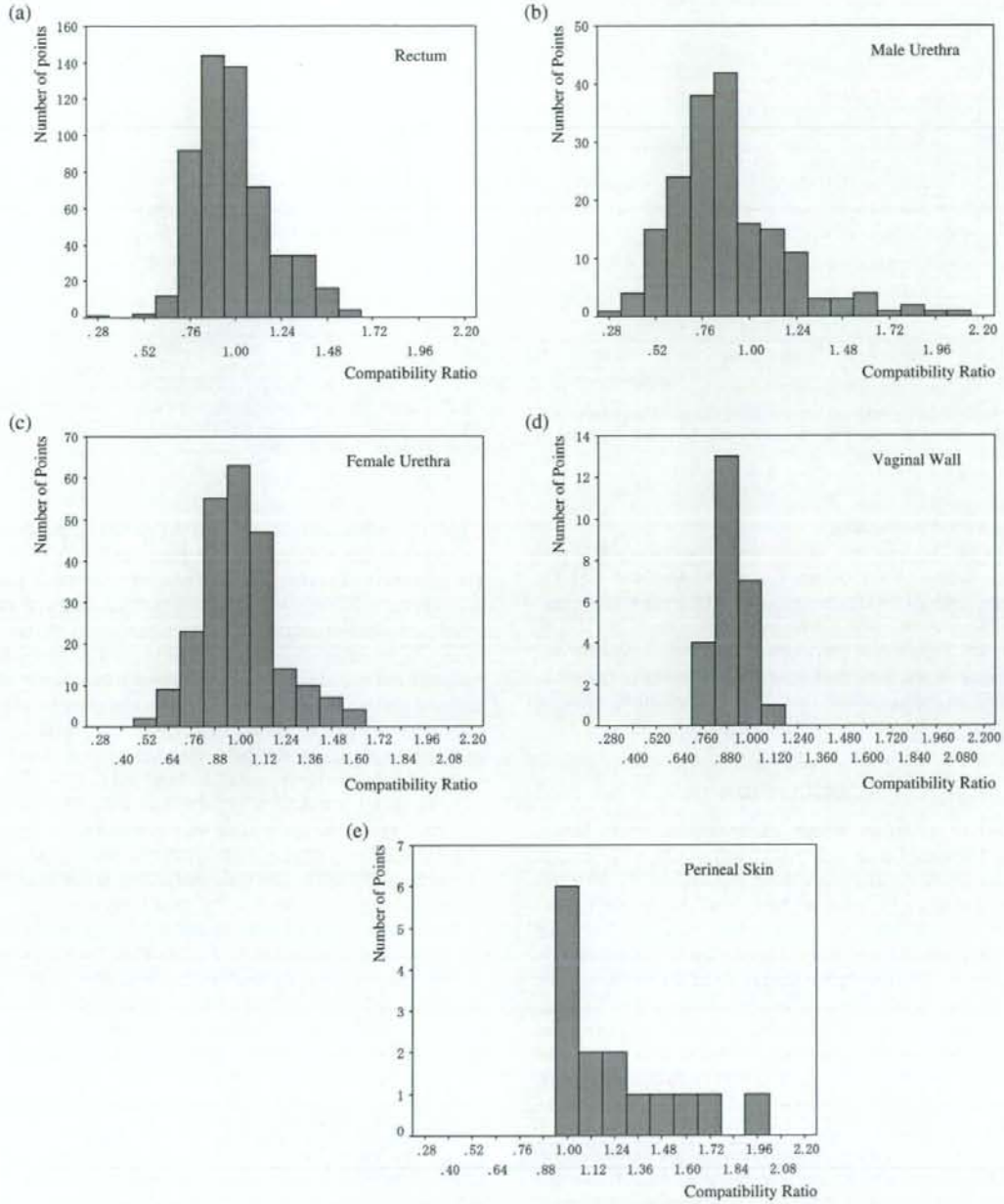

Fig. 3. (a) Frequency of compatibility ratio for radiophotoluminescence glass dosimeter (RPLGD) for the rectum. Abscissa: ratio of measured dose/calculated dose. Ordinate: number of points for RPLGDs. Distribution approximates Gaussian, with mean compatibility of 0.99 ± 0.20. (b) Frequency of compatibility ratio for RPLGD for the male urethra. Abscissa: ratio of measured dose/calculated dose. Ordinate: number of RPLGDs. Distribution is positive-skewed and negatively shifted, with mean compatibility of 0.90 ± 0.30. (c) Frequency of compatibility ratio for RPLGD for the female urethra. Abscissa: ratio of measured dose/calculated dose. Ordinate: number of RPLGDs. Distribution approximates Gaussian, with mean compatibility of 1.01 ± 0.20. (d) Frequency of compatibility ratio for RPLGD for the vaginal wall. Abscissa: ratio of measured dose/calculated dose. Ordinate: number of points for RPLGDs. Distribution is negatively shifted steep Gaussian, with mean compatibility of 0.91 ± 0.08. (e) Frequency of compatibility ratio for RPLGD for the perineum. Abscissa: ratio of measured dose/calculated dose. Ordinate: number of RPLGDs. Distribution is positive-skewed and with mean compatibility of 1.25 ± 0.32.

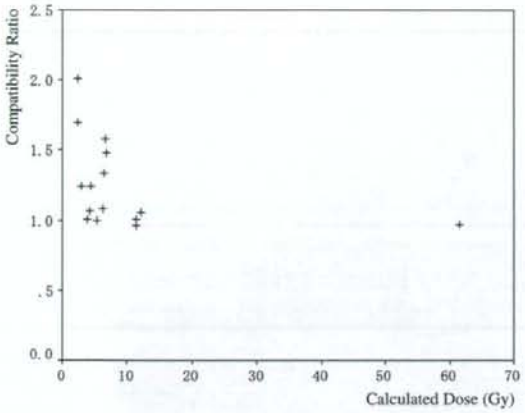

Fig. 4. Correlation between compatibility ratio (ordinate; measured dose/calculated dose) and the calculated dose (abscissa) for perineal skin.

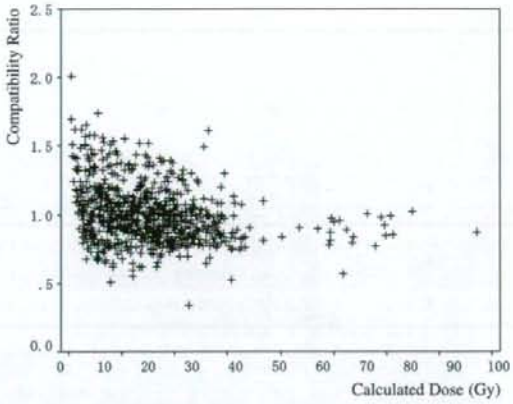

Fig. 5. Correlation between compatibility ratio (ordinate; measured dose/calculated dose) and the calculated dose (abscissa) for 823 points (male urethra excluded).

Dose for the perineal skin

For the 15 dosimeters, the median measured and calculated doses were 6.85 Gy (range, 3.65–59.62 Gy) and 6.33 Gy (range, 2.42–61.64 Gy), respectively. The compatibility ratio of the measured and calculated doses was 1.25 ± 0.32 (Fig. 3e). Transit dose plays an important role in positive discrepancy of the measured dose and its impact is known to depend on the calculated dose (21). Compatibility ratio according to calculated dose is displayed in Fig. 4.

DISCUSSION

In vivo dosimetry studies for interstitial brachytherapy have previously dealt only with small numbers of patients, except for pioneering work using RPLGDs at the Veterans Administration Hospital in New York in the 1950s and 1960s (5–9, 13). To the best of our knowledge, this is the largest *in vivo* dosimetry study conducted for interstitial brachytherapy. The simple handling of RPLGDs facilitates their routine use in clinical situations; in addition, their linearity and reproducibility are better than those of the TLDs used previously (5–9). Measured doses in this study were contaminated by simulation X-rays; data with excessive contamination were excluded by setting a threshold for measured doses.

For male urethral measurements, suturing of the catheter to the urethral orifice did not eliminate the migration of dosimeters that prevents precise data from being obtained. For female urethral measurements, this technique eliminated migration. The frequency for compatibility of measured and calculated doses displayed a wide Gaussian distribution, with mean 1.01 ± 0.20. For the rectum, compatibility displayed a similar Gaussian distribution (0.99 ± 0.20). These deviations (±20%) are attributable to the movements for these organs independent of movement for the target, and hence for the applicators. In our previous *in vivo* dosimetry study for 61 head and neck brachytherapy patients, the compatibility for nontarget organs (the submandibular skin and the mandible) displayed a wider Gaussian distribution, with mean 1.06 ± 0.32 (12). The movement of nontarget organs relative to the applicators is less in the pelvic region (where target organs and applicators do not move voluntarily) than in the head and neck region (where target organs move under the control of voluntary muscles). For nontarget organs in the pelvic region, actual absorbed doses can be 20% greater than calculated doses, compared with 32% in the head and neck region. Lead shielding is an effective protection that halves the absorbed dose to the nontarget organs in the region of the head and neck (4); however, shielding is impractical for the rectum and urethra during interstitial brachytherapy. Actual dose monitoring for organs at risk is feasible by employing an alternative real-time dosimeter such as MOSFET (22). If excessive dose is detected, the initial planning can be adapted for subsequent sessions.

For the target (vaginal wall), compatibility displayed a narrow Gaussian distribution (0.91 ± 0.08). This 8% deviation is the smallest among all the locations and is similar to the 10% deviation (0.95 ± 0.10) observed for the head and neck target in our previous study (12). Movement of the target is synchronized with the applicators, provided that the applicators are implanted in the target, irrespective of the target type and movement pattern (pelvis, nonvoluntary movement by surrounding organ volumes; head and neck, voluntary movement). The 9% negative shift is attributable to the lack of inhomogeneity correction in the software for the vaginal cylinder, which has a density of 1.24. The acceptable criteria for brachytherapy, as stated by the Radiological Physics Center, is 15% (23), which is achievable using inhomogeneity correction. Use of a real-time dosimeter is desirable to achieve more precise delivery of the planned dose.

The transit dose affects all the measured doses to some degree. The importance of the transit dose depends on calculated dose (21). As shown in Fig. 4, the calculated dose seems to affect the compatibility ratio for the perineal skin.

The compatibility ratio approaches unity as the calculated dose increases, especially for >10 Gy. For 823 points (excluding male urethral points), 294 points were to receive calculated dose <10 Gy, and the compatibility ratio was 1.09 ± 0.25, whereas 529 points were to receive calculated dose ≥10 Gy, and the compatibility ratio was 0.97 ± 0.18 ($p < 0.001$) (Fig. 5). Transit dose should be incorporated in points with calculated dose <10 Gy, although the clinical impact of these low doses remains unclear.

In conclusion, the compatibility ratio of the measured and calculated doses for the target displayed a small deviation (8%) caused by synchronized movement with the applicators, and a 9% negative shift attributable to the cylinder material. The addition of inhomogeneity correction to the planning software would enable the acceptable criteria for the target of brachytherapy (15%) to be easily achieved. The transit dose should be incorporated into points with a calculated dose of <10 Gy. Measured doses for organs at risk displayed as much as 20% deviation from the planned doses because of involuntary movements. The next step to using these findings will be to establish an adaptive dose delivery system using a real-time dosimeter.

REFERENCES

1. Lachance B, Béliveau-Nadeau D, Lessard É, *et al.* Early clinical experience with anatomy-based inverse planning dose optimization for high-dose-rate boost of the prostate. *Int J Radiat Oncol Biol Phys* 2002;54:86–100.
2. Sumida I, Shiomi H, Yoshioka Y, *et al.* Optimization of dose distribution for HDR brachytherapy of the prostate using attraction-repulsion model. *Int J Radiat Oncol Biol Phys* 2006;64: 643–649.
3. Nose T, Peiffert D, Lapeyre M, *et al.* Clinical target volume-based dose specification for interstitial brachytherapy: Minimum target dose comparison with classical implant system. *J Brachyther Int* 2001;17:345–353.
4. Nose T, Koizumi M, Nishiyama K. High-dose-rate interstitial brachytherapy for oropharyngeal carcinoma: Results of 83 lesions in 82 patients. *Int J Radiat Oncol Biol Phys* 2004;59: 983–991.
5. Mangold CA, Rijnders A, Georg D, *et al.* Quality control in interstitial brachytherapy of the breast using pulsed dose rate: Treatment planning and dose delivery with an Ir-192 afterloading system. *Radiother Oncol* 2001;58:43–51.
6. Brezovich IA, Duan J, Pareek PN, *et al.* In vivo urethral dose measurements: A method to verify high dose rate prostate treatments. *Med Phys* 2000;27:2297–2301.
7. Hamers HP, Johansson KA, Venselaar JLM, *et al.* In vivo dosimetry with TLD in conservative treatment of breast cancer patients treated with the EORTC protocol 22881. *Acta Oncol* 1993;32:435–443.
8. Anagnostopoulos G, Baltas D, Geretschlaeger A, *et al.* In vivo thermoluminescence dosimetry dose verification of transperineal ^{192}Ir high-dose-rate brachytherapy using CT-based planning for the treatment of prostate cancer. *Int J Radiat Oncol Biol Phys* 2003;57:1183–1191.
9. Kälkner KM, Bengtsson E, Eriksson S, *et al.* Dosimetry of anal radiation in high-dose-rate brachytherapy for prostate cancer. *Brachytherapy* 2007;6:49–52.
10. Tsuda M. A few remarks on photoluminescence dosimetry with high energy X-rays. *Jpn J Med Phys* 2000;20:131–139.
11. Araki F, Ikegami T, Ishidoya T, *et al.* Measurements of Gamma-Knife helmet output factors using a radiophotoluminescent glass rod dosimeter and a diode detector. *Med Phys* 2003;30: 1976–1981.
12. Nose T, Koizumi M, Yoshida K, *et al. In vivo* dosimetry of high-dose-rate brachytherapy: Study on 61 head-and-neck cancer patients using radiophotoluminescence glass dosimeter. *Int J Radiat Oncol Biol Phys* 2005;61:945–953.
13. Roswit B, Malsky SJ, Reid CB, *et al.* In vivo radiation dosimetry. Review of a 12-year experience. *Radiology* 1970;97:413–424.
14. Perry JA. Luminescence phenomena. In: Perry JA, editor. RPL dosimetry. Radiophotoluminescence in health physics. Bristol, United Kingdom: IOP; 1987. p. 1–7.
15. Perry JA. Instrumentation and technique. In: Perry JA, editor. RPL dosimetry. Radiophotoluminescence in health physics. Bristol, United Kingdom: IOP; 1987. p. 141–160.
16. Japan Society of Medical Physics, editor. Standard dosimetry of absorbed dose in external beam radiotherapy (Standard Dosimetry 01). Tokyo: Tsuusyou Sangyou Kenkyu; 2002 [in Japanese].
17. Leung S. Perineal template techniques for interstitial implantation of gynecological cancers using the Paris System of dosimetry. *Int J Radiat Oncol Biol Phys* 1990;19:769–774.
18. Dutreix A, Marinello G, Wambersie A. Dosimétrie du système de Paris. In: Dutreix A, Marinello G, Wambersie A, editors. Dosimétrie en curiethérapie. Paris: Masson; 1982. p. 109–138.
19. Siegel S. In: Nonparametric statistics for the behavioral sciences. New York: McGraw-Hill; 1956.
20. Kaplan EL, Meier P. Nonparametric estimation for incomplete observation. *J Am Stat Assoc* 1958;53:457–511.
21. Thomadsen BR, Houdek PV, van der Laarse R, *et al.* Treatment planning and optimization. In: Nag S, editor. High dose rate brachytherapy: A text book. Armonk, NY: Futura; 1994. p. 79–145.
22. Cygler JE, Saoudi A, Perry G, *et al.* Feasibility study of using MOSFET detectors for in vivo dosimetry during permanent low-dose-rate prostate implants. *Radiother Oncol* 2006;80: 296–301.
23. Hanson WF, Shalek RJ, kennedy P. Dosimetry quality assurance in the U.S. from the experience of the Radiological Physics Center. In: Starkschall G, Horton J, editors. Quality assurance in radiotherapy physics. Madison, WI: Medical Physics; 1991. p. 255–282.